NEUROSCIENCE
RESEARCH ARTICLE
J. Vera et al. / Neuroscience 426 (2020) 13–32

Modulation of Frequency Preference in Heterogeneous Populations of Theta-resonant Neurons

Jorge Vera,[†] Ulises Pereira[‡] Bryan Reynaert Juan Bacigalupo and Magdalena Sanhueza[*]

Department of Biology, Faculty of Sciences, University of Chile. Las Palmeras 3425, Santiago, Chile

Abstract—Neurons from several brain regions resonate in the theta frequency range (4–12 Hz), displaying a higher voltage response to oscillatory currents at a preferred 'resonant' frequency (f_R). Subthreshold resonance could influence spiking and contribute to the selective entrainment of neurons during the network oscillatory activity that accompanies several cognitive processes. Neurons from different regions display resonance in specific theta subranges, suggesting a functional specialization. Further experimental work is needed to characterize this diversity and explore how frequency preference could be dynamically modulated. Theoretical studies have shown that the fine-tuning of resonance depends in a complex way on a variety of intrinsic factors and input properties, but their specific influence is difficult to dissect in cells. We performed slice electrophysiology, dynamic clamping and modelling to assess the differential frequency preference of rat entorhinal stellate neurons, hippocampal CA1 pyramidal neurons and cortical amygdala neurons, which share a hyperpolarization-activated current (I_h)-dependent resonance mechanism. We found heterogeneous resonance properties among the different types of theta-resonant neurons, as well as in each specific group. In all the neurons studied, f_R inversely correlated with the effective input resistance (R_{in}), a measurable variable that depends on passive and active membrane features. We showed that resonance can be adjusted by manipulations mimicking naturally occurring processes, as the incorporation of a virtual constant conductance or cell depolarization, in a way that preserves the f_R-R_{in} relationship. The modulation of frequency selectivity influences firing by shifting spike frequency and timing, which could influence neuronal communication in an active network.

Key words: theta-frequency resonance, frequency modulation, input resistance, resonant frequency, phase-lag, spike timing.

INTRODUCTION

Theta frequency waves (4–10 Hz) emerge in the brain from the coordinated rhythmic neuronal electrical activity (Buzsáki, 2006; Colgin 2013) thought to underlie cognitive processes like active sensory sampling, navigation and learning (Kay, 2005; Lisman and Buzsáki, 2008; Mizuseki et al., 2009; Ranade et al., 2013). These waves spread across different neuronal networks, supporting a code based on the frequency and timing of neuronal firing (Lisman and Jensen, 2013; Wilson et al., 2015; Lopes-dos-Santos et al., 2018).

Neurons from several brain regions display subthreshold frequency preference (resonance) in the theta range in response to stimulation with oscillatory currents. Examples of theta-resonant neurons are estellate cells from the entorhinal cortex (SL) (Erchova et al., 2004), pyramidal neurons from the CA1 hippocampus (HP) (Hu et al., 2002) and resonant neurons from the olfactory amygdala (AM) (Vera et al., 2014). This frequency selectivity can involve the amplitude and the phase lag of the voltage responses to the oscillatory inputs. Amplitude resonance occurs when neurons respond with an increased voltage oscillation at frequencies near a preferred, non-zero frequency, called the resonant frequency (f_R), and is characterized by a peak in the impedance amplitude profile (impedance vs. frequency curve) at such frequency (Hutcheon and Yarom, 2000). The impedance phase (Φ) is the lag of the voltage response relative to the oscillatory input; zero-phase resonance (or phasonance) occurs when the impedance phase of the response is zero at a non-zero (phase-resonant) frequency (f_p; Richardson et al., 2003; Rotstein, 2014, 2017a). This means that for this frequency, the temporal delay between the current stimulus (input) and the voltage response (output) is zero and both signals fluctuate synchronously. For frequencies bellow the phase-resonant frequency, the voltage oscillation

*Corresponding author. Address: Department of Biology, Faculty of Sciences, University of Chile, Las Palmeras 3425, Ñuñoa 7800024, Santiago, Chile.
E-mail address: masanhue@uchile.cl (M. Sanhueza).
[†] Present address: Dominick Purpura Department of Neuroscience, Albert Einstein College of Medicine, Bronx, NY, USA.
[‡] Present address: Department of Statistics, The University of Chicago, Chicago, IL, USA.

https://doi.org/10.1016/j.neuroscience.2019.10.054
0306-4522/

may precede the oscillatory current (negative Φ). Frequency preference is an emergent property that arises from the interaction between the time scales of neuronal biophysical properties and the time scales of the oscillatory stimulus (Rotstein, 2014).

Subthreshold theta resonance depends in part on intrinsic neuronal features arising from the orchestration of active and passive membrane properties, in which the core active component is an ionic current that produces a slow negative feedback effect on membrane potential fluctuations at frequencies below ~12 Hz (Hutcheon and Yarom, 2000; Richardson et al., 2003; Rotstein and Nadim, 2014). In cortical neurons, the membrane currents that participate in subthreshold frequency preference in the theta range are the hyperpolarization-activated current (I_h) and, in some cases as HP neurons, the muscarine sensitive current (I_M), at depolarized voltages. According to their voltage sensitivity, I_h underlies resonance in the hyperpolarized subthreshold range, but in SL and AM cells it generates frequency selectivity at perithreshold voltages (while I_M produces resonance around threshold in CA1 neurons (more positive than ~ -60 mV) (Hu et al., 2002). The ionic currents that have a positive feedback effect on the membrane potential, like the voltage-dependent persistent sodium conductance (I_{NaP}) (French et al., 1990), do not generate resonance by themselves, but can amplify the resonant effect and modulate their properties, including the values of the resonance and phasonance frequencies (Hutcheon and Yarom, 2000; Rotstein and Nadim, 2014). I_{NaP} contributes to the amplification of oscillatory responses near its activation voltage (positive to ~ -65 mV) and may regulate the expression of I_M-dependent subthreshold resonance (Vera et al., 2017).

In order to have a role in neural processing, subthreshold resonance should influence action potential firing. The communication of subthreshold theta resonance to firing depends on the interplay between the currents implicated in the subthreshold regime and those involved in spiking. *In vitro* experiments and modeling have shown that subthreshold resonance evoked by oscillatory stimulation can dictate the firing probability for low input amplitudes that allow the voltage responses to reach spike threshold around f_R. This phenomenon is termed evoked spiking resonance and has been observed theoretically (Hutcheon et al., 1996a; Rotstein, 2017a), as well as experimentally (Erchova et al., 2004; Vera et al., 2014, 2017; but see Stark et al., 2013). If theta-band subthreshold frequency preference influences the firing probability *in vivo*, it may contribute to the selective activation of neurons by coordinated oscillatory synaptic inputs around a particular frequency. Thus, resonance could promote the recruitment of resonant cells to dynamic oscillating assemblies (Schmidt et al., 2017; but see Stark et al., 2013). The joint effort of *in vivo* and *in vitro* works, as well as theoretical studies, may shed light on whether subthreshold resonance could influence neuron computation in an active brain.

The mechanisms underlying subthreshold theta-resonance and phasonance have been characterized experimentally and theoretically in several brain areas. Experimental approaches usually address resonance in specific regions or subregions and characterize neuron responses by showing sample results and average measures (see refs. above). Moreover, an important body of theoretical studies have investigated frequency preference and their possible influence on spiking, by considering the behavior of model neurons. These studies have shown how subthreshold and spiking resonance, as well as phase response, change upon modifications of intrinsic biophysical parameters, membrane potential or simulated synaptic activity (Hutcheon et al., 1996a; Richardson et al., 2003; Rotstein and Nadim, 2014). A question arising from these observations is how the inherent variability of biological systems influences theta resonant behavior in a cell type and among neurons from different brain regions. Further experimental studies are required to address this issue and to evaluate the factors that could modulate frequency preference in both subthreshold and firing regimes.

Experimental evidence indicates that theta-resonant neurons from the mammalian brain exhibit heterogeneous preferred frequencies, with values ranging from 2 to 15 Hz: 3–15 Hz in the isocortex (Gutfreund et al., 1995; Hutcheon et al., 1996b), 2–4 Hz in the thalamus (Puil et al., 1994), 2–5 Hz in the hippocampus (Hu et al., 2002), 5–15 Hz in the entorhinal cortex (Erchova et al., 2004; Giocomo et al., 2007), 2–6 Hz in the amygdala (Pape and Driesang, 1998; Vera et al., 2014) and 3–7 Hz in the olfactory bulb (Hu et al., 2016), suggesting that the frequency selectivity of neurons spans a wide range of values, including frequencies beyond the theta range. Many factors can contribute to this heterogeneity of frequency preference, like neuronal size and morphology and the differential expression and distribution of the voltage-dependent currents involved in subthreshold resonance, among others. Additional factors that could have influenced these results are methodological: resonant parameters are highly sensitive to the experimental conditions (temperature, pipette solution, intracellular recording technique, among others), raising the question of whether the described heterogeneity reflects real biological variability or whether it is partly due to different experimental conditions.

Theoretical approaches indicate that f_R depends on the passive membrane resistance (R_m; Puil et al., 1986; Hutcheon et al., 1996a; Rotstein and Nadim, 2014), suggesting that the physiological variability of R_m could be one of the causes behind the observed diversity of f_R values, and that natural fluctuations of R_m might modulate resonance in individual cells (an idea first proposed by Hutcheon et al., 1996a). It has been difficult to experimentally address the dynamical link between f_R and R_m, in part because the measurement of R_m is hampered by the presence of other membrane conductances, whose voltage- and time-dependent activation deviates the voltage behavior from the purely passive response (Spruston and Johnston, 1992; Surges et al., 2004; Ceballos et al., 2017). Moreover, the axial current flux associated to a complex neuronal morphology also deviates the membrane response from that of

the ideal electrocompact neuron (Golowasch et al., 2009). The input resistance (R_{in}), also known as the effective input resistance, is determined from the steady-state deflection of the membrane potential induced by a square current pulse. For small voltage perturbations, the R_{in} of a spherical cell depends on passive and synaptic currents and on the steady-state activation of voltage-dependent conductances (Puil et al., 1986; Surges et al., 2004). Therefore, R_{in} is determined by a diverse set of cell's intrinsic parameters and external factors, and it is expected that fluctuations in these biophysical properties will affect its value, as is the case for f_R and Φ. Interestingly, the induction of synaptic potentiation in hippocampal CA1 pyramidal neurons caused upregulation of HCN1 channels carrying I_h, with a consequent increase in f_R and a correlated decrease in R_{in} and neuron excitability, as measured at the soma and along the apical dendrites (Narayanan and Johnston, 2007).

Here, we experimentally characterized the diversity of resonance properties (f_R and Φ) in SL, HP and AM neurons, that share an I_h-dependent mechanism at hyperpolarized potentials and display heterogeneous frequency preference in the theta band. We compared resonance features among the different cell populations and in each specific group. We addressed how resonance relates to R_{in} along the whole population and evaluated if controlled changes in membrane conductance and potential that modify R_{in} within physiological ranges, are capable of significantly varying the frequency tuning of individual cells and in what frequency band. We restricted our study to input amplitudes low enough to maintain the cells in a linear regime that could allow the subthreshold frequency preference to influence the firing regime (Rotstein, 2017a; but see Hutcheon et al., 1996b).

We found that, when measured in the same experimental conditions, these cells display clear differences in R_{in}, f_R, and phase profiles, as well as in resonance strength and impedance amplitude. We observed that the biological diversity of resonant properties correlates to the natural variability in R_{in}, with f_R-R_{in} values following a negative power-law distribution that contains all tested cells, generating a continuum of f_Rs along the theta range. Moreover, upon modifications in R_{in} in individual cells within physiological ranges, f_R fluctuated constrained to the theta band, following the f_R-R_{in} relationship. We show that, in individual cells, changes in R_{in} generated within physiological ranges, followed the same f_R-R_{in} relationship constrained to the theta frequency band. This modulation is observed in the spike frequency and timing, suggesting that natural fluctuations of membrane conductance could influence the frequency preference that the neurons express and communicate to other neurons downstream. Considering previous theoretical and experimental approaches, we analyzed the results of these experiments as a whole including other resonance attributes, and explored the factors contributing to resonance diversity and modulation.

EXPERIMENTAL PROCEDURES

Ethical approval

Animal care and experimental procedures were approved by the Bio-Ethical Committee of the Faculty of Sciences, University of Chile, according to the ethical rules of the Biosafety Policy Manual of the National Fund for Development of Science and Technology (FONDECYT).

Slice preparation

Male Sprague Dawley rats (18–30 days-old) were deeply anesthetized with isoflurane, decapitated and their brain was rapidly removed and transferred to an ice-cold dissection solution containing (in mM): 206 sucrose, 2.8 KCl, 1 $MgCl_2$, 2 $MgSO_4$, 1 $CaCl_2$, 26 $NaHCO_3$, 1.12 NaH_2PO_4, 10 glucose and 0.4 ascorbic acid (equilibrated with 95% O_2 and 5% CO_2), pH 7.3. Slices (400 μm) containing the region of interest were obtained with a vibratome (Vibratome Sectioning System 102, Pelco) using standard disposable stainless-steel razor blades (www.personna.com). For the anterior nucleus of the cortical amygdala we used coronal slices targeting the region between Bregma −2.2 and −3.3 (Sanhueza and Bacigalupo, 2005; Vera et al., 2014). For hippocampal neurons we used septotemporal slices targeting the dorsal hippocampus (Vera et al., 2017) and for stellate cells we used horizontal slices to target the dorsomedial entorhinal cortex (Giocomo et al., 2007). Slices were placed in a holding chamber with standard artificial cerebro-spinal fluid (ACSF) and were let to recover at least 1 h at 30 °C before using them for recording.

Electrophysiological recordings

Whole cell patch-clamp recordings were conducted under visual guidance in an upright microscope (Nikon Eclipse E600FN) equipped with DIC optics. Patch pipettes (3.5–4.5 MΩ) were fabricated of borosilicate glass with a horizontal puller (Flaming/Brown P-97, Sutter Instrument Co). Current-clamp recordings were made with an EPC-10 patch-clamp amplifier (Heka, Heidelberg, Germany), data were filtered at 5 kHz and acquired at 40 kHz using the Patch Master software from Heka. All experiments were performed at 34 ± 2 °C, and in the presence of 10 μM CNQX and 100 μM PTX, to block AMPA-R and GABAa-R mediated currents, respectively.

Recording solutions (in mM)

Artificial cerebro-spinal solution (ACSF) contained (in mM): 124 NaCl, 2.8 KCl, 1.25 NaH_2PO_4, 26 $NaHCO_3$, 10 Glucose, 2 $MgCl_2$, 2 $CaCl_2$ and 0.4 ascorbic acid (equilibrated with 95% O_2 and 5% CO_2), pH 7.3 and 290 mOsm.

Internal pipette solution contained (in mM): 123 K-Gluconate, 10 KCl, 4 Glucose, 1 EGTA, 10 HEPES, 2 Na_2ATP, 0.2 Na_3GTP, 10 phosphocreatine-Na or -TRIS, 1 $MgCl_2$, 0.1 $CaCl_2$, pH 7.35 and 290 mOsm. This composition was based on previous works reporting stability of intrinsic excitability parameters (Xu et al.,

2005; Kaczorowski et al., 2011), corroborated in investigations related to intrinsic frequency preference (Vera et al., 2014, 2017). We measured the liquid junction potential (LJP) between pipette solution and ACSF (~13 mV) according to the procedure described by Neher (Neher, 1992) and used this value to correct the data in offline analyses.

ZAP stimulation and data analysis

The ZAP (impedance amplitude profile) stimulus consisted in a pseudo-sinusoidal current of constant amplitude and linearly increasing frequency from 0 to 20 Hz in 10 s (ZAP stimuli). The protocol was repeated 8 to 10 times in every neuron and the membrane voltage waves were averaged for the impedance analysis. The impedance profile ($Z(f)$) and phase-lag ($\Phi(f)$) curves were obtained from the ratio of the Fast Fourier Transforms (FFT) of the output (voltage) and input (current) waves ($Z(f) = FFT[V(t)]/FFT[I(t)]$). The impedance is a complex quantity ($Z(f) = Z_{Real} + iZ_{Imaginary}$), where Z_{Real} is the resistive component of the impedance and $Z_{Imaginary}$ the reactive component. For each given frequency, the complex impedance can be plotted as a vector whose magnitude and phase ($\Phi(f)$; angle with the real axis) are respectively given by the following expressions:

$$|Z|(f) = \sqrt{Z^2_{Real}(f) + Z^2_{Imaginary}(f)} \quad (1)$$

$$\Phi(f) = tan^{-1}\left(\frac{Z_{Imaginary}(f)}{Z_{Real}(f)}\right) \quad (2)$$

The term *impedance* is used throughout the text to refer to the magnitude of the impedance vector, unless otherwise stated. The impedance phase corresponds to the phase shift of the voltage wave relative to the current wave. Frequencies below 0.2 Hz were not plotted in the impedance and phase profiles graphs, to avoid low frequency distortions. Data analysis was performed using Igor Pro 6.37 software (Wavemetrics.com).

To maintain the system in linear conditions, we used low amplitude ZAP stimuli (20–100 pA) in order to produce oscillations of ~5 mV (peak-to-peak). In principle, f_R could be different if the stimulus frequency increased or decreased. To check if the R_{in}-f_R relationship was independent of the direction of frequency change we used our model neurons (see below), to explore f_R at different R_{in} values for increasing (0–20 Hz) or decreasing (20–0 Hz) frequencies. In both conditions, the obtained f_R range was identical (5–11 Hz, average 6.4 Hz).

Quantification of resonance

We measured the preferred frequency (f_R) of each neuron as the frequency at which the impedance amplitude reached the peak ($|Z_{Max}|$). Resonance strength was quantified with the Q value, measured as the ratio between the maximal impedance ($|Z_{Max}|$) and the impedance at 0.5 Hz ($|Z(0.5)|$) (Hutcheon et al., 1996b). For a more precise determination of f_R and Q, the experimental data were fitted with a polynomial curve between 0.2 and 15 Hz and the peak value was calculated. For simplicity, throughout the text we refer to $|Z_{Max}|$ as Z_{Max}.

Dynamic clamp experiments

For the dynamic-clamp experiments, the current-clamp amplifier was driven by an analog signal from a dual core desktop computer running the Real-Time Experimental Interface, RTXI (Dorval et al., 2001), using an update frequency of 25 KHz.

The somatic conductance was altered by simulating a virtual constant conductance G to be added or subtracted from the cell via the dynamic clamp, to mimic changes in the leak conductance G_{Leak}. The injected current I was computed according to the following equation:

$$I = G(V_m - E_{Leak}) \quad (3)$$

where V_m is the online recorded membrane potential and E_{Leak} is the reversal potential (set to −70 mV). For $G > 0$, R_{in} decreases and for $G < 0$, R_{in} increases.

Figs. 3 and 5 display dynamic currents (I_{DynC}) as the external currents that were injected, following the standard convention that positive currents are depolarizing and negative currents are hyperpolarizing. Therefore,

$$I_{DynC} = -I \quad (4)$$

Computer simulations

We developed a minimal point process and conductance-based model following the Hodgkin-Huxley formalism (Hodgkin and Huxley, 1952). The model includes a membrane capacitance (C_m), a passive leak current (I_{Leak}), the hyperpolarization-activated h current, I_h (Spain et al., 1987) and an external stimulating current, I_{ZAP} (Hutcheon et al., 1996b). As this basic model will be used for hyperpolarized membrane potentials (−80 mV), it does not include other active currents that may affect resonance, such as the voltage-dependent persistent sodium conductance (I_{NaP}). Similarly, the model does not include a firing mechanism (fast sodium and potassium conductances).

The equation describing the evolution of the membrane potential (V) in time is

$$C_m\frac{dV}{dt} = I_{ZAP} - I_{Leak} - I_h \quad (5)$$

where C_m is the membrane capacitance and I_{ZAP} is the externally applied current. The intrinsic ionic currents in Eq. (5) are described by the following equations:

$$I_{Leak} = G_{Leak}(V - E_{Leak}) \quad (6)$$

$$I_h = G_h w(V - E_h) \quad (7)$$

where G_{Leak} and G_h are the maximal conductances of the corresponding currents and E_{Leak} (−65 mV) and E_h (−40 mV) are the reversal potentials of I_{Leak} and I_h, respectively, and w is the state variable of I_h. Since theoretical work has shown that the omission of slow gating variables has little effect on oscillatory dynamic of resonant neurons (Rotstein, 2017b), in our minimal model

Table 1. The parameters G_h and G_{Leak} were adjusted to reproduce the experimental values of R_{in}, f_R, Φ_{6Hz} and Φ_{fR}. C values were estimated from the experiments

Model cell	C (pF)	G_h (nS)	G_{Leak} (nS)	R_{in} (MΩ)	f_R (Hz)	Φ_{6Hz} (deg)	Φ_{fR} (deg)
SL	160	$0.06*C_m$	$0.1*C_m$	30	8.9	−1.5	−10.6
HP	120	$0.025*C_m$	$0.08*C_m$	66	6.1	−13.5	−14.8
AM	80	$0.013*C_m$	$0.04*C_m$	190	3.9	−31.5	−17.5

we only use the fast component of I_h. The fast gating variable is that related to theta resonance and accounts for ∼80% of the total current (Spain et al., 1987).

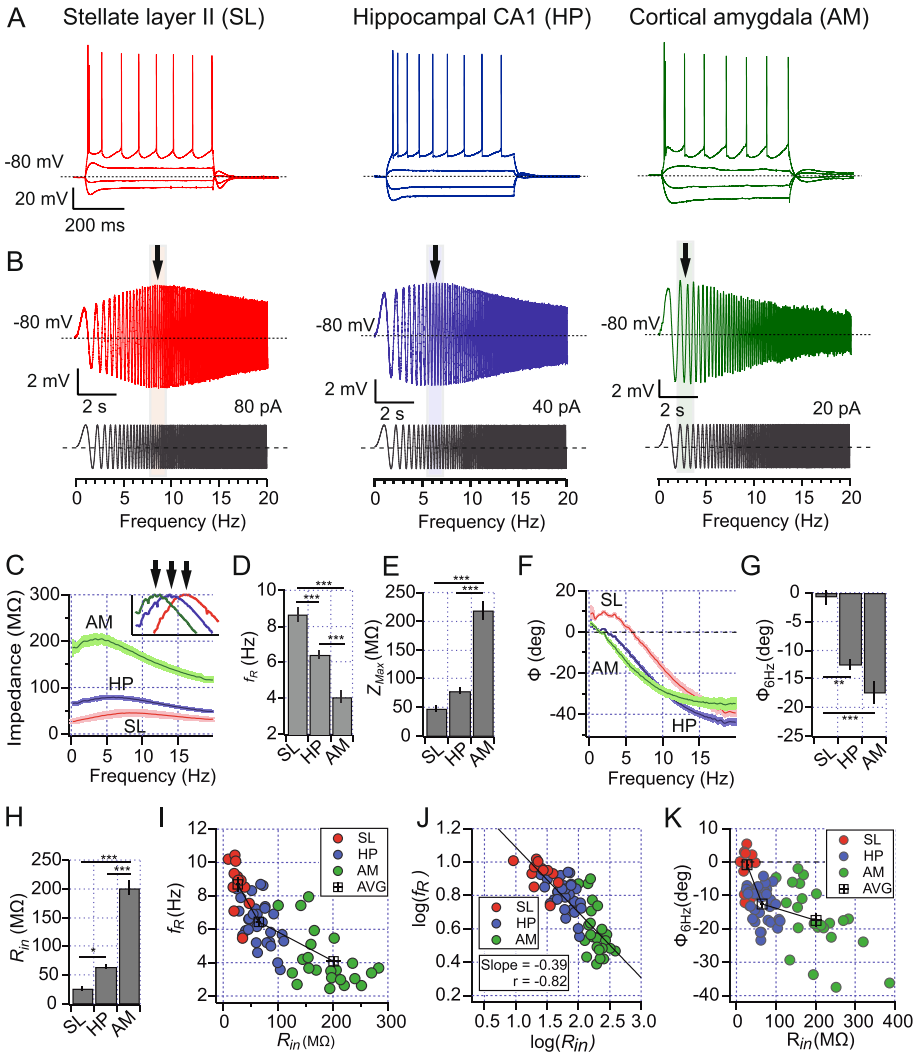

Fig. 1. Frequency preference of resonant cell types correlates with their R_{in}. Impedance and phase analysis performed in SL (n = 12), HP, (n = 31) and AM, (n = 25) neurons. (**A**). Representative voltage responses of SL (red), HP (blue) and AM (green) neurons to current pulses (−150, −50, +100, +150 pA for SL, −200, −100, +50, +100 pA for HP and −100, −50, +50, +100 pA for AM neurons). (**B**). Representative voltage responses of each cell type to ZAP stimulation (grey traces, see Experimental procedures). Peak voltage responses are indicated with arrows. (**C**). Impedance profiles of each cell type (dark and light colors depict mean and SEM, respectively); the inset shows normalized average curves from 0.8 to 1 (y axes) and from 0 to 14 Hz (x axes). Arrows show the peak of each curve. (**D**). Average f_R of each cell type. (**E**). Average peak impedance (Z_{Max}) of each cell type. (**F**). Φ curves, dark and light colors depict mean and SEM, respectively. (**G**). Quantification of phase-lag at 6 Hz (Φ_{6Hz}). (**H**). R_{in} of SL, HP and AM neurons measured at −80 mV with a hyperpolarizing square pulse. (**I**). Scatter plots of f_R vs. R_{in} with data from all recorded neurons (n = 68). (**J**). Scatter plot of log(f_R) vs. log(R_{in}). (**K**). Scatter plot of Φ_{6Hz} vs. R_{in}. One way ANOVA and Tukey's multiple comparison tests, * = P < 0.05, ** = P < 0.01, and *** = P < 0.001.

The dynamics of the state variable w is ruled by the following equation:

$$\frac{dw}{dt} = \frac{w_\infty(V) - w}{\tau_w(V)} \quad (8)$$

where τ_w is the time constant and w_∞ is the steady-state value of w, calculated according to:

$$w_\infty = \frac{1}{1 + e^{(V+78)/7}} \quad (9)$$

τ_w was set to 0.05 s, similar to the fast component described by Spain et al. (Spain et al., 1987), to match the exact f_R range observed in our experiments.

We constructed a computer model for each cell type by introducing the membrane capacitance estimated from voltage-clamp recordings (50 ms, 5 mV pulse). G_h and G_{Leak} were the only parameters that we slightly tuned in order to reproduce average R_{in}, Z_{Max}, f_R, Q and phase-lag curves of each cell type (Table 1). To explore the effects of G_{Leak}, we considered values from 1 to 80 nS.

Simulations were performed using Igor Pro 6.37 software with an integration time step of 10 μs. The code for reproducing the computer simulations described in this paper is available upon request to authors.

Statistical analysis

The statistical analysis was performed using GraphPad Prism 6.07 (GraphPad Software, Inc, USA) or Igor Pro 6.37 (Wavemetrics.com). Group data is presented as the mean ± standard error. We used different parametric tests for data with normal distribution (Z_{Max}, f_R, Vm, R_{in}, Φ_{6Hz} and Φ_{fR} passed normality and equal variance tests). When the data structure was a single variable measured at the same membrane potential and compared between different cell types (Fig. 1,

Table 2. Electrophysiological parameters of SL, HP and AM neurons at hyperpolarized potentials. Mean ± SEM. Pairs comparison: 1 SL-HP, 2 SL-AM and 3 HP-AM. Statistics summary one-way ANOVA with Tukey's multiple comparison tests: (s) = $P < 0.05$ and (ns) $P \geq 0.05$. Vm $F(2,65) = 2.04$ $P = 0.14$, Z_{Max} $F(2,65) = 65.19$ $P < 0.0001$, f_R $F(2,65) = 43.11$ $P <$ 1e-4, Φ_{6Hz} $F(2,65) = 22.07$ $P <$ 1e-4, and Φ_{fR} $F(2,65) = 21.7$ $P <$ 1e-4. Q value Kruskal–Wallis test $\chi^2(2,65) = 33.63$ $P <$ 1e-4 (For details on statistics see Experimental procedures)

	V_m (mV)	Z_{Max} (MΩ)	f_R (Hz)	Q	Φ_{6Hz} (deg)	Φ_{fR} (deg)	n
SL	−79.6 ± 0.4	48 ± 6.1	8.7 ± 0.4	1.62 ± 0.05	−0.7 ± 1.5	−12.4 ± 0.6	12
HP	−80.0 ± 0.6	78 ± 5.0	6.5 ± 0.3	1.23 ± 0.02	−12.6 ± 0.1	−13.9 ± 0.6	31
AM	−80.6 ± 0.3	220 ± 16.2	4.1 ± 0.3	1.15 ± 0.02	−17.5 ± 0.8	−8.4 ± 0.7	25
Stats	(ns)	1(ns),2(s),3(s)	1(s),2(s),3(s)	1(s),2(s),3(ns)	1(s),2(s),3(s)	1(ns),2(s),3(s)	

Table 2), we used one-way ANOVA and Tukey's multiple comparison tests. When the data structure was a single variable measured from the same cells but comparing different membrane potentials (Fig. 2, Table 3), we used Repeated measures one-way ANOVA and Tukey's multiple comparison tests. When the comparison of variables was between two conditions in the same cell (Fig. 3), we used paired Student's *t*-test. To evaluate the shift in firing probability ($F_{P0.5}$) after reducing R_{in} (Fig. 4), we used Wilcoxon matched-pairs signed rank test, while the change in phase-lag was evaluated using paired Student's *t*-test. The statistical significance of the linear relation between $\log(f_R)$ and $\log(R_{in})$ (Figs. 1 and 2) was evaluated with a Student test. When comparing Q values, we used a non-parametric Kruskal–Wallis test for unpaired data (Tables 2), and Friedman test with

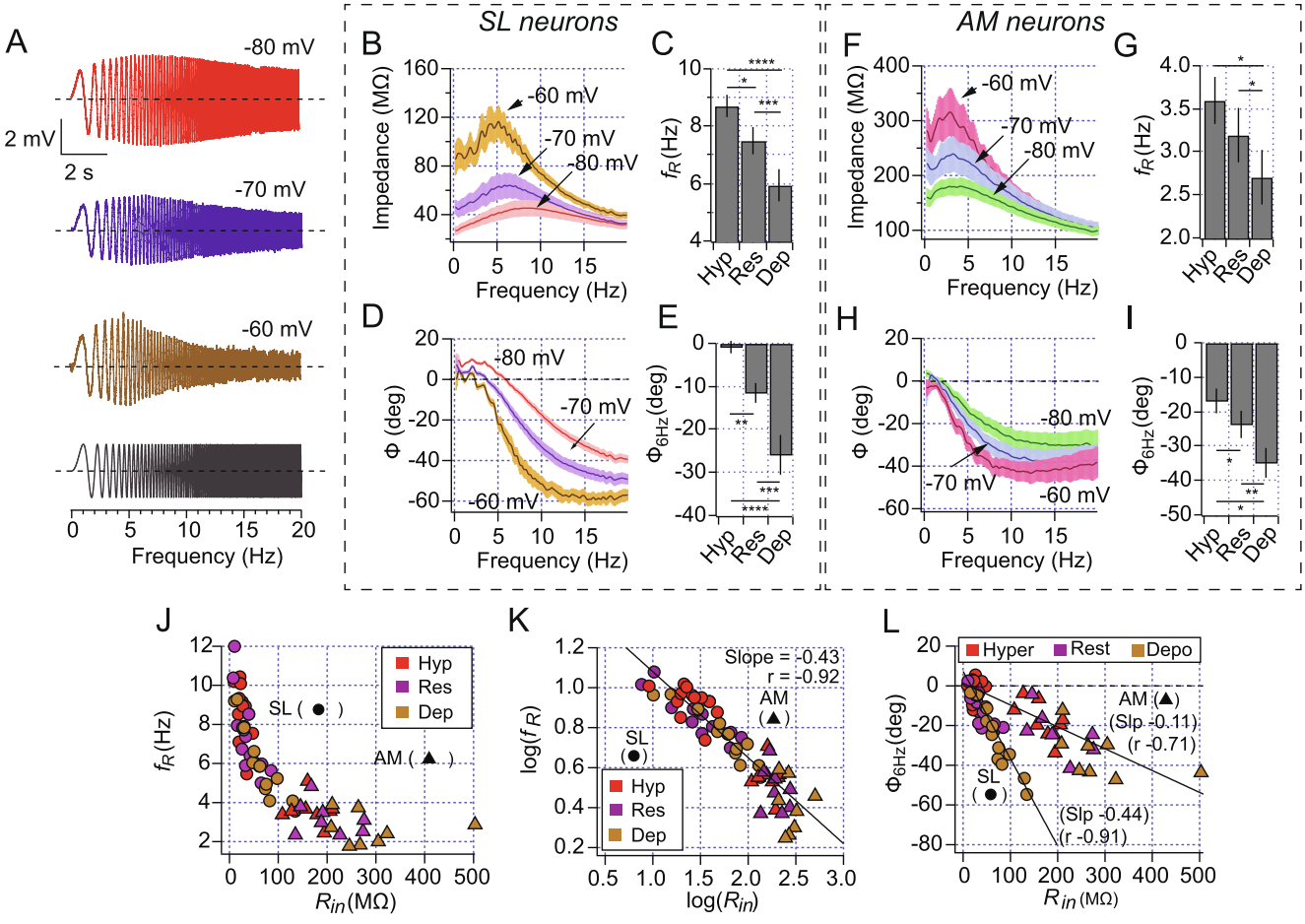

Fig. 2. Reduction in f_R and increment in Φ during depolarization-driven increase in R_{in}. Measurement of resonant properties in SL ($n = 12$) and AM ($n = 8$) neurons recorded at hyperpolarized (Hyp), resting (Res) and depolarized (Dep) membrane potentials (see Table 3). (**A**). Representative voltage responses of a SL neuron to ZAP stimuli. The amplitude of the sinusoidal current (gray trace) was adjusted to maintain voltage oscillations near 5 mV (in this example, 40, 20 and 5 pA for −80, −70 and −60 mV, respectively). (**B**). Impedance profiles of SL neurons (mean ± SEM). (**C**). Quantification of f_R as a function of membrane potential for SL neurons. (**D**). Φ curves for SL neurons. (**E**). Quantification of Φ at 6 Hz for SL neurons. (**F-I**). Same as **B-E** for AM neurons. (**J**). Scatter plot of f_R vs. R_{in} for the pooled data from SL and AM neurons. Colors indicate the voltage of SL (circles) and AM (triangles) neurons. (**K**). Scatter plot of $\log(f_R)$ vs. $\log(R_{in})$. Labels as in J. (**L**). Scatter plot of Φ_{6Hz} vs. R_{in} from the pooled data of SL and AM neurons. All neurons were recorded at the three voltages. Repeated measures one way ANOVA and Tukey's multiple comparison tests, * = $P < 0.05$, ** = $P < 0.01$ and *** = $P < 0.001$ and **** = $P < 0.0001$. Traces in B–E and F–I are mean ± SEM.

Table 3. Intrinsic electrophysiological parameters for SL and AM neurons, obtained for hyperpolarized (Hyp), near-resting (Res) and depolarized (Dep) potentials. Mean ± SEM. Pairwise comparison (1) Hyp-Res, (2) Hyp-Dep and (3) Res-Dep. Statistics summary repeated measures one way ANOVA with Tukey's multiple comparison tests: (s) = $P < 0.05$ and (ns) $P \geq 0.05$. SL neurons: R_{in} $F(1.305,14.36) = 26.68$, $P <$ 1e-4; Z_{Max} $F(1.153,12.68) = 30.23$, $P < 0.001$; f_R $F(1.33,14.66) = 27.09$, $P < 0.001$; Φ_{6Hz} $F(1.15,12.65) = 24.69$, $P =$ 2e-4; and Φ_{fR} $F(1.54,16.95) = 15.18$, $P =$ 4e-4; Q Friedman test $\chi^2(2,11) = 11.79$, $P = 0.0028$. AM neurons: Repeated measures one way ANOVA R_{in} $F(1.10,7.72) = 16.93$, $P = 0.0032$; Z_{Max} $F(1.04,7.28) = 12.25$, $P = 0.009$; f_R $F(1.47,10.32) = 13.47$, $P = 0.002$; Φ_{6Hz} $F(1.29,9.05) = 20.26$, $P = 0.001$; and Φ_{fR} $F(1.54,10.79) = 2.26$, $P = 0.16$; Q Friedman test $\chi^2(2,7) = 1.41$, $P = 0.56$ (For details on statistics see Experimental procedures)

		V_m (mV)	R_{in} (MΩ)	Z_{max} (MΩ)	f_R (Hz)	Q	Φ_{6Hz} (deg)	Φ_{fR} (deg)	n
SL	Hyp	−79.6 ± 0.4	26.5 ± 2.9	47.9 ± 5.7	8.7 ± 0.4	1.62 ± 0.04	−0.7 ± 1.4	−12.4 ± 0.6	12
	Res	−68.6 ± 0.8	36.2 ± 6.1	56.7 ± 9.0	7.5 ± 0.5	1.49 ± 0.06	−11.4 ± 2.3	−16.7 ± 0.1	12
	Dep	−61.6 ± 0.4	65.5 ± 10.3	106.1 ± 18.1	6.0 ± 0.5	1.43 ± 0.12	−25.8 ± 4.5	−19.6 ± 1.6	12
Stats			1(s),2(s),3(s)	1(s),2(s),3(s)	1(s),2(s),3(s)	1(s),2(s),3(ns)	1(s),2(s),3(s)	1(s),2(s),3(s)	
AM	Hyp	−80.6 ± 1.8	167.5 ± 13.9	182.2 ± 17.3	3.6 ± 0.3	1.16 ± 0.04	−17.0 ± 3.7	−7.4 ± 1.9	8
	Res	−75.8 ± 1.8	200.3 ± 20.3	226.7 ± 23.5	3.2 ± 0.3	1.17 ± 0.03	−23.7 ± 4.1	−8.6 ± 2.0	8
	Dep	−63.6 ± 1.1	290 ± 35.8	312.7 ± 44.5	2.7 ± 0.3	1.22 ± 0.06	−34.8 ± 4.4	−10.2 ± 1.5	8
Stats			1(s),2(s),3(s)	1(s),2(s),3(s)	1(ns),2(s),3(s)	ns	1(s),2(s),3(s)	ns	

Dunn's multiple comparisons test for paired data (Table 3). Statistical tests were two-tailed and we used $\alpha = 0.05$ as critic value. Statistic results are informed as the statistic's value (degrees of freedom within parenthesis) and the P value.

RESULTS

High variability of resonant properties within and between cell types is correlated with the membrane input resistance

We first addressed the question of how heterogeneous are the resonant properties of different types of cortical neurons and whether this variability might be related to the natural heterogeneity of R_{in} values. We chose to conduct whole cell recordings from SL, HP and AM resonant cell types because they differ in their reported resonant frequency range, they share an I_h-dependent resonant mechanism at hyperpolarized potentials and also because of their differences in R_{in} range (Hu et al., 2002; Erchova et al., 2004; Vera et al., 2014). Fig. 1A shows the voltage responses of representative neurons of each type to hyperpolarizing and depolarizing square current pulses. In each of them the responses to both stimuli polarities start with a sag at the onset of the pulse, produced by the slow (tens of milliseconds) activation or deactivation of the inward I_h, respectively (Biel et al., 2009). At the end of the pulse, there is a transient rebound with similar kinetics (Biel et al., 2009). Further depolarization induced trains of action potentials with some frequency accommodation, presumably due to I_h deactivation and the activation of the muscarine sensitive potassium current (I_M) (Peters et al., 2005). The comparison of their intrinsic behaviors shows that these cell types have comparable hyperpolarized voltage responses to square current pulses and similar firing patterns, belonging to the cell category of regular spiking (Contreras, 2004).

To quantify and compare the resonant properties of these neurons, we recorded their voltage responses to oscillatory current stimulation. We applied ZAP (impedance amplitude profile) stimuli (Puil et al., 1986), consisting of a 10 s oscillatory current of constant amplitude and linearly incremental frequencies, from 0 to 20 Hz. The membrane potential was manually adjusted to ∼−80 mV to set a similar level of activation of I_h. The stimulus amplitude, ranging from 10 to 50 pA, was adjusted to produce a comparable voltage deflection of ∼5 mV peak-to-peak at its onset, in order to maintain the system in linear conditions. As expected (Hutcheon and Yarom, 2000), the voltage response in all tested cells displayed a maximal amplitude in the theta range (arrows), while at lower and higher frequencies their responses were attenuated (Fig. 1B).

The average impedance profiles of the three groups of neurons were clearly different. Their characteristic shapes resemble band-pass filters with peaks in the theta range (Fig. 1C), although their impedance curves are displaced in the frequency range, as can be better appreciated in the normalized impedance profiles (Fig. 1C, inset). The f_Rs derived from the impedance curves were higher in SL (8.7 ± 0.4 Hz, $n = 12$) than in HP (6.5 ± 0.3 Hz; $n = 31$) and AM neurons (4.1 ± 0.3 Hz, $n = 25$; $P < 0.001$ for all paired comparisons; one way ANOVA $F(2,65) = 43.11$; Table 2, Fig. 1D). Related to membrane impedances, the average maximal impedances (Z_{Max}) were clearly dissimilar, with ∼50 MΩ for SL, ∼80 MΩ for HP and ∼220 MΩ for AM neurons ($F(2,65) = 65.19$; $P < 0.0001$; Table 2, Fig. 1E). The resonance strength among the different cell populations, evaluated using the Q value (see Experimental procedures), was also different among these cell types ($\chi^2(2,65) = 33.63$; $P < 0.0001$; Table 2).

We also studied the Φ of the voltage response to evaluate the heterogeneity in the temporal response of the cells. Φ curves quantify the delay of the output voltage wave relative to the input current stimulus as a function of frequency (Rotstein, 2014). Negative values of Φ reflect a delay of the voltage response, while positive values mean an advance of the output signal, providing important insights of the temporal processing of oscillatory stimuli by resonant neurons (Rotstein, 2014). The comparison of Φ showed a shorter lag at frequencies within and below the theta range (0–8 Hz) for SL in comparison to HP and AM neurons (Fig. 1F). To quantify and compare the Φ of each cell type, we measured it at two relevant frequencies: at the middle of theta range (6 Hz,

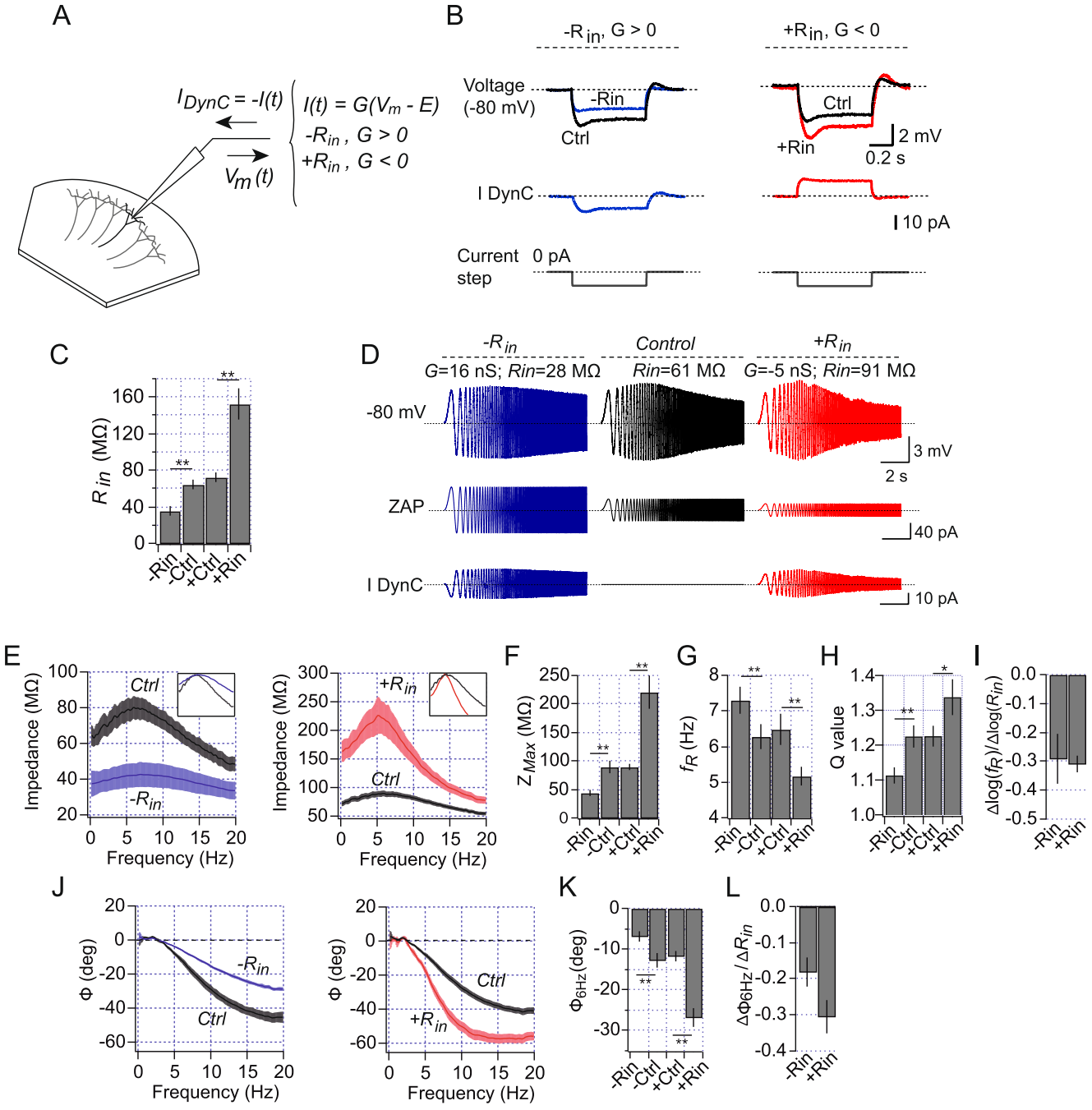

Fig. 3. Changes in the passive conductance modulate resonance frequency preference of CA1 hippocampal neurons. (**A**). R_{in} changes were generated with dynamic-clamp, as shown in the diagram. The neuron R_{in} was decreased ($-R_{in}$) or increased ($+R_{in}$) by injecting a virtual positive ($+G$) or negative ($-G$) somatic conductance by application of an external dynamic current (I_{DynC}). (**B**). Dynamic-clamp experiment showing the attenuation ($-R_{in}$) or amplification ($+R_{in}$) of voltage responses to 0.4 s and 50 pA hyperpolarizing pulses (gray). At the $-R_{in}$ condition, I_{DynC} is negative (blue trace), hyperpolarizing the neuron and attenuating the voltage response. At $+R_{in}$, I_{DynC} is positive (red trace), depolarizing the cells and amplifying the voltage deflections. (**C**). Quantification of R_{in} for the conditions $-R_{in}$ and $+R_{in}$, and for their respective controls without conductance injection. R_{in} was measured with a square pulse whose amplitude was adjusted to evoke a ~4 mV voltage deflection in all conditions. The R_{in} change was set to attain a reduction of ~45% ($G = 16.6 \pm 2.9$ nS, $n = 10$) or an increase in ~100% ($G = -6.1 \pm 0.8$ nS, $n = 10$). (**D**). Representative experiment showing the oscillatory responses at different R_{in} values. Both conditions were explored in the same cell. ZAP stimulation was applied at control (black), $-R_{in}$ (blue) or $+R_{in}$ (red) conditions. (**E**). Impedance profiles (mean ± SEM) for $-R_{in}$ and $+R_{in}$, with their respective control curves. The insets show normalized profiles. (**F**). Peak impedance for $-R_{in}$, $+R_{in}$ and control conditions. (**G**). Same as F, for f_R. (**H**). Same as F, for the *Q* value. (**I**). Ratio between Δlog (f_R) and Δlog (R_{in}), for $-R_{in}$ and $+R_{in}$. (**J**). Φ curves for $-R_{in}$ and $+R_{in}$, with their respective control curves. (**K**). Phase-lag at 6 Hz (Φ_{6Hz}) for $-R_{in}$ and $+R_{in}$. (**L**). $\Delta\Phi_{6Hz}/\Delta R_{in}$ for $-R_{in}$ and $+R_{in}$ conditions. ** = $P < 0.01$, Paired Student's *t*-test.

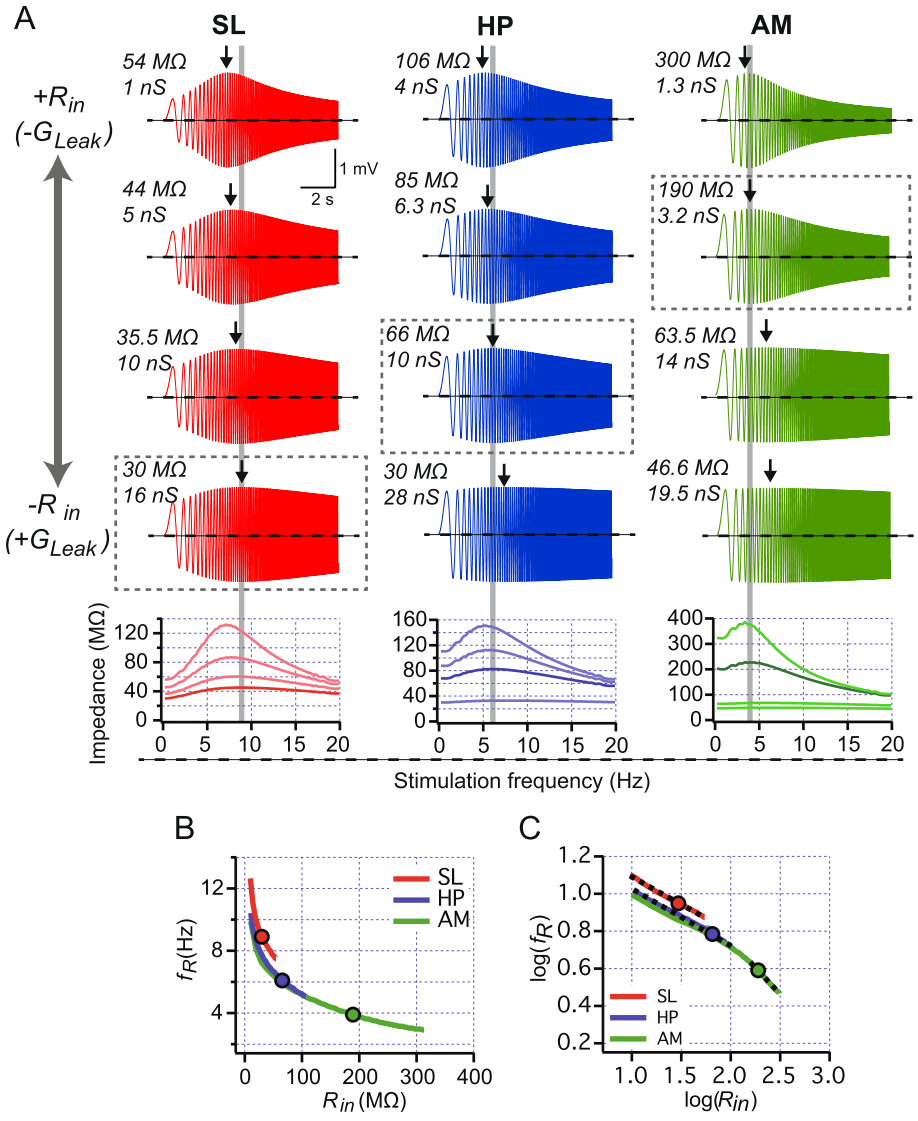

Fig. 4. Modulation of subthreshold frequency preference along the theta range by changes in G_{Leak} in the three cell types. (**A**). Representative SL, HP and AM neurons were simulated using a minimal resonant model (see Experimental procedures). Starting with G_{Leak} and G_h values that reproduced the average f_R, R_{in} and phase-lag of each cell type (i.e. control conditions, dotted boxes), we explored voltage responses ranging G_{Leak} from ~1 nS ($+R_{in}$) to 80 nS ($-R_{in}$), while maintaining constant G_h and C_m. Four conditions are shown for each cell type, R_{in} and G_{Leak} are reported at the top left of each voltage trace. The impedance profile plots are shown at the bottom, with the darker curve corresponding to the control condition. Grey bars show the values of f_R at control condition, while arrows show the f_R for each simulated voltage trace. The amplitude of the oscillatory current was adjusted to produce voltage responses of ~2 mV peak-to-peak and a DC current was injected to hyperpolarize the model cells to −80 mV. (**B**). Plot of f_R vs. R_{in} obtained with the exploration of G_{Leak} in the three cell types (colored lines), with filled circles showing values at control condition. (**C**). Same as B for log(f_R) vs. log(R_{in}). Dotted black lines are the linear fit of each curve, with a slope of −0.29 (SL), −0.31 (HP) and −0.57 (AM).

Φ_{6Hz}) and at the f_R of each particular neuron (Φ_{fR}). The average Φ_{6Hz} values were markedly different between the three groups: −0.7 ± 1.5 deg, −12.5 ± 1.0 deg and −17.5 ± 2.0 deg for SL, HP and AM neurons, respectively (Fig. 1G, Table 2; $P < 0.001$ in all paired comparisons, one way ANOVA $F(2,65) = 22.07$; $P < 0.0001$). By transforming these lag values from degrees to time (where 360 deg are 166.7 ms in a single oscillation at 6 Hz), we obtain a lag of −0.3 ms, −5.8 ms and −8.1 ms for SL, HP and AM neurons, respectively. These differences in the temporal response might be relevant in these cell types for the timing of spikes generated under oscillatory stimulation. When Φ is compared at the respective f_Rs, the three neurons display less variability than at 6 Hz, with values that are still different but grouped in the narrow range of 8–14 deg (Table 2).

These results show that, under the same experimental conditions, the three resonant neuron types display different f_R and Φ, confirming that they have heterogeneous frequency preference in the theta frequency band. We aimed to address the basis of this variability. As resonance depends on the passive membrane resistance (Hutcheon et al., 1996a; Hutcheon and Yarom, 2000; Rotstein and Nadim, 2014), and the comparison of impedance profiles showed clear differences in the maximal membrane impedance among the three cell types, we first investigated the relationship between resonant parameters and the input resistance R_{in} at hyperpolarized membrane potentials. We measured R_{in} as the steady state deflection in the membrane potential during a 250 ms hyperpolarizing current pulse from −80 mV, whose amplitude was adjusted to produce a ~5 mV maximal deflection. R_{in} values of the three types of neurons ranged from 10 to 400 MΩ, being SL neurons more abundant in the lower (mean = ~26 MΩ), HPs in the intermediate (mean = ~65 MΩ) and AMs in the highest R_{in} subranges (mean = ~200 MΩ; Fig. 1H, statistics in Table 2).

For a more detailed examination of relationship between f_R and R_{in}, we built a scatter plot with the values from all recorded cells. We found a negative correlation, as f_R increased as R_{in} decreased. Low-R_{in} cells show the highest f_Rs, while the lowest f_Rs were observed in the high-R_{in} cells (Fig. 1I). The R_{in} range covered by the cells is associated with a continuous variation of f_Rs from about 2 to 10 Hz, with the frequencies of each cell group spanning the ranges previously reported for these theta-resonant neurons. Since the distribution of the data in the scatter plot

seems to represent a multiplicative relationship between f_R and R_{in}, we transformed the data to logarithmic values (Kass et al., 2014). The scatter plot of log(f_R)-log (R_{in}) pairs yields a linear relationship characterized by a Pearson's correlation coefficient of −0.82 and a slope of −0.39 (n = 68; P < 0.001), suggesting a power law dependence between f_R and R_{in} (Fig. 1J).

We also explored the relationship between Φ_{6Hz} and R_{in} by pooling the data from all cells in a scatter plot. Φ_{6Hz} is also correlated with R_{in}, dominating the values around zero lag for lower R_{in} cells, while for higher R_{in} the phase values can reach up to ∼−40 deg (Fig. 1K).

This comparative analysis revealed a co-variation range for resonant parameters (f_R and Φ_{6Hz}) and the physiological R_{in} value measured at −80 mV in heterogeneous populations of resonant neurons. In linear conditions, the f_R- R_{in} relationship follows a power law spanning and limited to the theta range.

As R_{in} depends on active and passive membrane properties as for f_R and Φ, it is expected that changes in these properties would be accompanied by modifications in frequency selectivity.

Changes in resonant properties upon cell depolarization

We explored the relationship of resonance and phase with R_{in} when individual neurons undergo changes in the voltage-dependent currents. It is possible, changing the holding membrane potential with constant current injections, to manipulate both R_{in} and f_R, by modifying the steady-state activation of voltage-sensitive conductances, while keeping unaltered the passive membrane properties. Steady-state depolarization of the cortical neurons produces a reduction of I_h due to deactivation (Hutcheon et al., 1996b; Hu et al., 2002; Biel et al., 2009) and above −70 mV causes the activation of the persistent Na^+ current, I_{NaP}. Both modifications produce a voltage-dependent rise in R_{in} that has been observed previously in resonant neurons (Gutfreund et al., 1995; Hutcheon et al., 1996b) and characterized in detail more recently (Surges et al., 2004; Economo et al., 2014; Yamada-Hanff & Bean, 2015; Ceballos et al., 2017); we will refer to it as "depolarization-driven increase in R_{in}". Theoretical work has shown that, in a regime comparable to the depolarization-driven increase in R_{in}, the interaction of I_h and I_{NaP} produces nonlinear amplification of voltage responses that modifies resonant parameters in different ways (Rotstein, 2015). However, as in the previous experiments, we induced low-amplitude oscillations (< 5 mV peak-to-peak) and therefore, the deviations from a linear regime are expected to be minor.

We evaluated the resonant properties of cortical neurons subjected to oscillatory stimulation at hyperpolarized, resting and depolarized potentials, and evaluated their relationship with R_{in}. We manually adjusted the membrane potential to −80, −70 and −60 mV by current injection and applied the ZAP stimuli at each potential, exploring R_{in} and resonance in SL and AM neurons. We did not include HP neurons in this experiment because they present a U-shaped voltage dependence of their f_R, lacking frequency preference between −70 and −65 mV (Hu et al., 2002; Vera et al., 2017).

The shape of the voltage responses to ZAP stimuli changed with depolarization, displaying a reduction in the f_R (Fig. 2A). Depolarization increased the average R_{in} from 26 to 65 MΩ in SL neurons (F(1.305,14.36) = 26.68; P < 0.0001) and from 167 to 290 MΩ in AM neurons (F(1.10,7.72) = 16.93; P = 0.0032), with an increase in peak impedance (Fig. 2B, F; Table 3). This increase in R_{in} was accompanied by a reduction in f_R from 8.7 to 6 Hz in SL neurons (F(1.33,14.66) = 27.09; P < 0.001, Fig. 2C, and from 3.6 to 2.7 Hz in AM neurons (F(1.47,10.32) = 13.47; P = 0.002, Fig. 2G, Table 3). The depolarization was also accompanied by a modification in Φ of both cell types, shifting the curves downward and leftward, with the consequent increment in lag as a function of frequency (Fig. 2D, H). The overall change in the Φ curves produced a considerable increase of Φ_{6Hz} in SL and AM neurons (−0.75 to −25.8 deg and −17.0 to −34.8 deg, respectively; Fig. 2E, I; see statistics in Table 3). When evaluated at f_R, Φ showed a smaller but significant range of variations under depolarization, increasing Φ_{fR} from −12 to −20 deg in SL neurons (F(1.54,16.95) = 15.18; P = 0.0004), while in AM neurons it stayed near −8 deg without significant changes (F(1.54,10.79) = 2.26; P = 0.16; see details in Table 3).

To explore the changes in f_R and phase-lag associated to the depolarization-driven increase in R_{in} in individual cells, we built scatter plots with the pooled data of f_R and Φ_{6Hz} vs. R_{in} from SL and AM neurons. R_{in} ranged from 10 to ∼100 MΩ in SL neurons and from 100 to ∼350 MΩ in AM neurons, filling the 10 to 350 MΩ R_{in} range almost completely (Fig. 2J). f_Rs inversely correlate with R_{in}, spanning the entire theta range. The distribution of f_R starts at 12 Hz for low-R_{in} SL neurons recorded at hyperpolarized potentials and decreases continuously to ∼2 Hz for high R_{in} AM neurons recorded at depolarized potentials (Fig. 2J). The distribution of f_R and R_{in} values strongly suggest a multiplicative relationship, as described above (Fig. 1). The log–log graph exhibits an even higher linear correlation, with a Pearson's coefficient of −0.92 and a slope of −0.43 (Fig. 2K; P < 0.001). These results agree with the R_{in}-f_R relationship between different cell types and show that f_R of individual neurons is coherently modified with changes in R_{in}.

The scatter plot of Φ_{6Hz} against R_{in} shows that neurons increment their Φ during the depolarization-driven increase in R_{in}, with both cell types spanning the whole range of 0 to −50 deg (Fig. 2L). This increase is dictated by linear trend of different slopes for each cell type (Pearson coefficient of −0.91 and −0.71 and slope of −0.45 deg/MΩ and −0.11 deg/MΩ for SL and AM neurons, respectively). Interestingly, despite having different R_{in} ranges and Φ curves, both cell types vary their Φ_{6Hz} along a similar range.

The activation/deactivation of voltage-dependent currents during cell depolarization (in the absence of

changes in passive properties) modified f_R and Φ, following the same correlation with R_{in} observed at hyperpolarized potentials among heterogeneous populations of resonant cells.

As proposed by theoretical studies, changes in the passive conductance or synaptic activity could operate as modulators of resonance (Hutcheon et al., 1996a; Richardson et al., 2003; Rotstein and Nadim, 2014). To address this question, we designed an experiment to modify the passive conductance while keeping mostly unaltered the contribution of the voltage-dependent conductances involved in resonance. We assessed the modulation of resonant properties constraining the changes in R_{in} to a physiological range.

Modulation of the frequency preference and phase-lag by controlled changes in membrane conductance

To explore how changes in the passive conductance in physiological ranges modulate resonance, we used the dynamic-clamp technique to add or subtract a virtual constant conductance G to the recorded neuron (Dorval et al., 2001; see Experimental procedures). Introduction or subtraction of this constant conductance can mimic an increase or decrease of leak ion conductance, which causes a decrease ($-R_{in}$, $G > 0$) or an increase ($+R_{in}$, $G < 0$) in R_{in}, respectively. This method allows to resemble more closely a physiological condition than the traditional procedure of injecting a constant current (Dorval et al., 2001). We performed these experiments in HP neurons at −80 mV, because at this voltage, R_{in} (∼70 MΩ), f_R and Φ values were at the middle of their dynamic range (see Fig. 1), facilitating the detection of positive and negative changes.

By manipulating the somatic conductance, we aimed to reduce or increase the R_{in} of HP neurons in order to match the average values of SL and AM cells, as examples of low and high-R_{in} cells, respectively (Fig. 3A, B). Using this criterion and setting the steady-state voltage to −80 mV, we generated a $-R_{in}$ condition with an average reduction of ∼45% compared to the respective control condition (-Ctrl) (from 63.8 ± 5.4 to 35.4 ± 4.8 MΩ; $T(9) = -7.51$; $P < 1e\text{-}4$; $G = 16.6 \pm 2.9$ nS, $n = 10$) and a ∼100% increment for a $+R_{in}$ condition, relative to +Ctrl (from 71.7 ± 4.7 to 151.8 ± 16.7 MΩ; $T(9) = -5.76$; $P < 5e\text{-}4$; $G = -6.1 \pm 0.8$ nS, $n = 10$, Fig. 3C). R_{in} values of both control groups were not different ($T(17.7) = 1.16$; $P = 0.13$, $n = 10$). These results demonstrate that our experimental procedure enabled us to change R_{in} over a wide physiological range, matching the values for the different cell types. We manually adjusted the membrane potential to −80 mV and recorded the control voltage responses to ZAP stimuli (Fig. 3D, black traces). Then, we reduced ($-R_{in}$, blue traces) or increased ($+R_{in}$, red traces) R_{in} with the dynamic clamp and recorded the voltage responses to oscillatory stimulation at the new level of somatic conductance. To keep the contribution of active properties at different R_{in} values approximately constant, we measured resonance systematically by adjusting the amplitude of the ZAP current to produce ∼5 mV peak-to-peak oscillations (measured at 4 Hz, Fig. 3D). In this way, we produced a comparable voltage oscillation in our different experimental conditions, recruiting a similar level of active currents. As expected, the manipulation of the somatic conductance generated changes in the impedance profile. In the $-R_{in}$ condition the impedance curve fell, with a Z_{Max} decrease of 50% (from 90 ± 10.2 to 44.1 ± 6.2 MΩ; $T(9) = 7.0$; $P = 6.3e\text{-}5$; Fig. 3E, F). In contrast, in the $+R_{in}$ condition the impedance curve increased (Fig. 3E), reaching a ∼150% increase of Z_{Max} (from 89.4 ± 5.1 to 221.6 ± 29.7 MΩ; $T(9) = -4.76$; $P = 0.001$; Fig. 3F).

The changes in peak impedance were accompanied by modifications in f_R. In the $-R_{in}$ condition, f_R decreased by ∼1 Hz (from 6.3 ± 0.4 to 7.3 ± 0.4 Hz,; $T(9) = -6.24$; $P = 1.5e\text{-}4$; Fig. 3G), while $+R_{in}$ was associated to a f_R decrease of ∼1.3 Hz (6.5 ± 0.4 vs. 5.2 ± 0.3 Hz; $T(9) = 4.77$; $P = 0.001$; Fig. 3G). The resonance strength was also modified, decreasing with respect to control for $-R_{in}$ (from 1.22 ± 0.03 to 1.13 ± 0.02; $P = 0.0098$, Wilcoxon signed-rank test) and increasing for $+R_{in}$ (from 1.23 ± 0.03 to 1.34 ± 0.05; ($P = 0.037$, Wilcoxon signed-rank test; Fig. 3H). To evaluate the magnitude of the resonance modulation, we calculated the ratio of the changes in the logarithms of f_R and R_{in} ($\Delta\log(f_R)/\Delta\log(R_{in})$) in each condition, obtaining values of −0.29 ± 0.09 and −0.31 ± 0.03 for $-R_{in}$ and $+R_{in}$ conditions, respectively (Fig. 3I). These values are similar to the slopes of the linear regression obtained for $\log(f_R)$-$\log(R_{in})$ when the source of R_{in} variation was the heterogeneity of SL, HP and AM neurons (Fig. 1K) or the depolarization-driven increase in R_{in} in SL and AM neurons (Fig. 2K). Therefore, by modifying R_{in} through changing only the passive somatic conductance it is possible to induce comparable variations in the frequency preference of the neurons.

As expected for changes in the membrane time constant, the manipulation of R_{in} also modified the Φ curve. The reduction of R_{in} produced a frequency-dependent reduction in phase-lag, with a ∼50% drop in Φ_{6Hz} (from −12.8 ± 1.7 to −6.8 ± 1.3 deg; $T(9) = -5.7$; $P = 2.9e\text{-}4$; Fig. 3J, K). Φ increased for $+R_{in}$, displaying a slower response at frequencies above 2 Hz (Fig. 3J), with a ∼130% increase in phase lag (Φ_{6Hz} changed from −11.7 ± 1.3 to −26.9 ± 2.3 deg; $T(9) = 6.95$; $P = 6.7e\text{-}5$; Fig. 3K). These variations give a rate of change in Φ_{6Hz} ($\Delta\Phi_{6Hz}/\Delta R_{in}$) of −0.18 ± 0.04 deg/MΩ and −0.31 ± 0.05 deg/MΩ for $-R_{in}$ and $+R_{in}$ conditions, respectively (Fig. 3L), between the values obtained for SL and AM neurons (Fig. 2L).

Taken together, these results indicate that by modifying exclusively the passive somatic conductance, to modulate R_{in} along the range of values of three populations, the changes in f_R followed the same trend and were confined to the same band observed in the conditions of Figs. 1 and 2. Our results agree with previous theoretical work that describes the dependence of resonant properties on the leak conductance (Rotstein and Nadim, 2014), and also show the restricted range of resonance properties that the neurons can explore *in vitro*. Moreover, these observations suggest

that individual neurons may adjust their frequency preference and temporal response in negative correlation with R_{in}, during massive conductance changes as those occurring upon intense synaptic inputs (Destexhe et al., 2003).

We next explored the range and properties of the modulation that the different cell types could undergo by the application of a constant conductance. We used a minimal conductance-based model containing only the hyperpolarization-activated conductance (G_h) as the resonant mechanism, that is active at −80 mV and is shared by the three cell types, a passive leak conductance (G_{Leak}) and a membrane capacitance (C_m). We first explored if it is possible to reproduce the differences in resonant properties displayed by average SL, HP and AM cells. We set the average value of C_m according to experimental observations and adjusted the magnitudes of G_h and G_{Leak} to reproduce the average values of R_{in}, f_R and Φ for each cell type, in accordance to the experimental values obtained by ZAP stimulation at −80 mV (Table 2). The characteristic voltage responses of the average model cells from each type are displayed in the dotted boxes of Fig. 4A (the values of the estimated biophysical parameters and the magnitudes of the reproduced resonance attributes are shown in Table 1). We explored the effects of changes in the passive conductance G_{Leak} in each of the three model neurons. As in the dynamic-clamp experiments (Fig. 3), we explored a reduction ($-R_{in}$) or an increase ($+R_{in}$) of the input resistance by gradually adjusting G_{Leak} between 1 and 80 nS. This manipulation varied the R_{in} of the model cells over the whole range of 10 to 310 MΩ. As expected, each simulated neuron changed its frequency preference as a result of G_{Leak} modifications. The shifts in conductance that generated a decrease in R_{in}, produced an increment in f_R in each cell type, with opposite effects for changes increasing R_{in} (in Fig. 4A, arrows indicate the f_R). Moreover, the f_R vs. R_{in} relationship obtained for each simulated cell type falls into the same curve, displaying the characteristic power-law distribution observed in our experimental data (Fig. 4B, C; filled circles correspond to the pairs f_R, R_{in} for the modelled average cell types). The lines represent simulations of the values of R_{in} and f_R attained by each single neuron when varied with slight consecutive increments in G_{Leak} (from 1 to 80 nS, 0.5 nS steps). In agreement with previous results, the log(f_R)-log(R_{in}) plot yields nearly linear curves in the three model cells, as described by a linear fit with slopes of −0.29 and −0.31 for the SL and HP models, respectively (Fig. 4C). In the case of the AM model, the log–log curve presents two regions of different slopes, of −0.25 below 2.0 Hz (similar to the HP model) and −0.57 above 2.0 Hz (Fig. 4C, dotted line above green line).

Overall, these computer simulations extend the results of the dynamic-clamp experiments to explore, for the whole population, the modulation of f_R by a passive conductance. Along with our experiments, they show that by these perturbations f_R can be adjusted in a range of frequencies that matches the theta spectrum, following the characteristic correlation with R_{in}.

Subthreshold frequency and phase modulation can be expressed as changes in spike frequency and timing

The influence of subthreshold resonance on action potential firing depends on the interaction of the ionic conductances active at subthreshold potentials and those involved in spiking. Evoked spiking resonance is observed when this interaction results in action potential firing around f_R, thus, when the firing frequency is dictated by subthreshold resonance (Rotstein, 2017a). This phenomenon has been described in SL, HP and AM neurons (Erchova et al., 2004; Vera et al., 2014, Vera et al., 2017; but see Stark et al., 2013).

A critical question is whether the modulation of subthreshold resonance is expressed in the spiking regime as a shift in the frequency at which evoked spiking resonance is observed. We tested this possibility by applying ZAP stimuli at perithreshold potentials and evaluating if experimental manipulations of R_{in} modified the spike firing probability and timing as predicted from the subthreshold results. These experiments were conducted in AM neurons because their high R_{in} and low f_R offer a wide range to reduce R_{in} and facilitate the detection of increases in firing frequency.

As in the previous experimental set, here we decreased R_{in} by recreating a constant membrane conductance with the dynamic clamp. As expected, this manipulation decreased the voltage responses, with the consequent reduction in cell excitability (Fig. 5A, left). In these experiments we set $-R_{in}$ by lowering it in ∼25 % (from 211 ± 27 to 163 ± 21 MΩ; $T(7) = 7.87$; $P = 1e\text{-}4$; $G = 1.8 \pm 0.46$ nS, $n = 8$; Fig. 5A, right). The neurons were depolarized to −60 mV and the amplitude of the oscillatory current was adjusted to reveal the preferential firing frequency, similar to the conditions in which evoked resonance is observed using low amplitude stimuli (Rotstein, 2017a). The stimulus consisted of a series of sinusoidal current pulses of constant amplitude with discrete increments in the frequencies between 0.5 and 14 Hz (Fig. 5B, blue traces). A representative example of an AM neuron response is shown in Fig. 5B (black trace). As expected, this neuron fired at frequencies of ∼2–4 Hz, with no action potentials at higher or lower frequencies. Interestingly, in the $-R_{in}$ condition the neuron changed its firing preference (red trace) to higher frequencies (6–8 Hz), with no action potentials in the lower range (2–4 Hz; Fig. 5C). To quantify the change in firing probability for the different stimulation frequencies, we computed a cumulative firing probability curve (cumulative probability density function, CPDF) for all recorded neurons (Fig. 5D; see Experimental procedures). These curves show that the reduction of R_{in} shifts the evoked firing probability towards higher frequencies, in agreement with the expected increase in the subthreshold f_R (Fig. 5D). The comparison of the frequencies at which the CPDF curves reached a probability of 0.5 ($F_{P0.5}$) reveals that the reduction of R_{in} produces a ∼2 Hz rightward shift in the evoked firing probability curve (from 3.8 ± 0.7 to 6.0 ± 0.8 Hz; Wilcoxon matched-pairs test, $P = 0.0078$; $n = 8$; Fig. 5E).

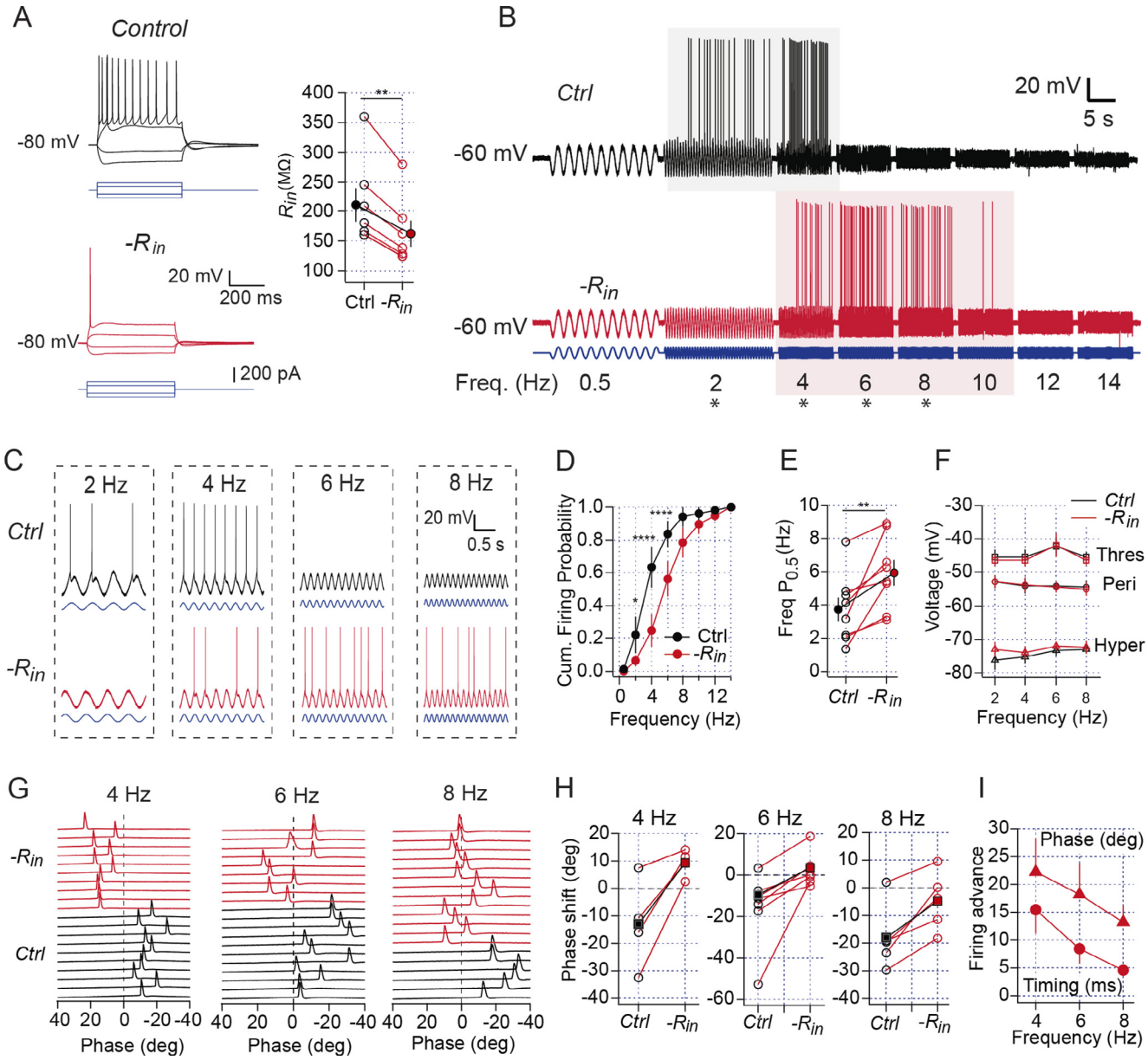

Fig. 5. Modulation of spiking resonance by adding a virtual constant somatic conductance. (**A**). Left, Voltage responses to depolarizing and hyperpolarizing current pulses of an AM neuron in control conditions (black) and after a 30% reduction in R_{in} by dynamic clamp (red; from 153 to 94 MΩ; see additional details in the text). Current pulses are the same in both conditions. Right, R_{in} values in a group of AM neurons (Control condition: black empty circles; $-R_{in}$ condition: red empty circles; $n = 8$), filled circles are mean ± SEM. (**B**). Voltage response of a resonant AM neuron under stimulation with an oscillatory current (blue) at control (black) and $-R_{in}$ (red) conditions. Stimulation protocol consisted of sequential sinusoidal waves of discrete frequencies: 0.5, 2, 4, 6, 8, 10, 12 and 14 Hz (each wave was applied during 10 s, with the exception of 0.5 and 2 Hz that lasted 20 s to sample more periods). Colored areas show the firing frequency range at each condition. (**C**). Time-scale amplification of the recordings in B labeled by asterisks (*). (**D**). Cumulative firing probability for control and $-R_{in}$ conditions ($n = 8$). (**E**). Frequency at which the firing probability is 0.5 ($P_{0.5}$; extracted from the curves in D) for both conditions (filled circles are the mean ± SEM). (**F**). Spike threshold (Thres), perithreshold (Peri) membrane potential (average of 10 ms window before spike threshold) and the peak of hyperpolarization during ZAP stimulation. (**G**). Representative recordings showing the phase shift of spikes fired at control (black lines) and $-R_{in}$ (red) conditions. The phase was calculated using the positive peak of sinusoidal current stimuli as a reference. (**H**). Phase shift in control and $-R_{in}$ conditions, filled black and red circles, respectively, are average values; Student t test, 4 Hz $T(3) = -3.66$ $P = 0.035$, 6 Hz $T(6) = -3.3$ $P = 0.016$, 8 Hz $T(6) = -3.8$ $P = 0.009$. (**I**). Firing advance quantified as the difference in phase shift between control and $-R_{in}$ conditions. * = $P < 0.05$, ** = $P < 0.01$, **** = $P < 0.0001$.

To discard that this firing modulation could have been generated by other changes, we compared the spike threshold, the voltage at which a spike is generated (the average in a 10 ms window before the spike threshold) and the peak of the hyperpolarization induced with the ZAP protocol (hyperpolarized potentials) for each spike fired in both conditions (control and $-R_{in}$, Fig. 5F). Neither of these parameters was different, suggesting that the voltage trajectory during oscillations and the activation of voltage-sensitive conductances was equivalent in control and $-R_{in}$ conditions. Therefore, the changes in firing frequency are most probably driven by

changes in f_R associated to the increase in somatic conductance.

To evaluate if modulating Φ influenced the timing of the spikes, we quantified the phase-shift of each spike relative to the peak of the sinusoidal current (see Experimental procedures). When the oscillatory current reached ~4–8 Hz, the AM neurons fired action potentials with average delays of −13 to −18 deg, the same range observed for the subthreshold Φ (Fig. 5G, black traces). We found that in the $-R_{in}$ condition the neurons consistently fired action potentials with a reduced delay at all tested frequencies (from −12.9 to 9.3 deg at 4 Hz, $T(3) = -3.7$; $P = 0.035$; from −9.5 to 3.5 deg at 6 Hz, $T(6) = -3.3$; $P = 0.016$; and from −17.9 to −11.4 at 8 Hz, $T(6) = -3.8$; $P = 0.009$; Fig. 5G, red traces and Fig. 5H). Note that at 4 Hz the reduction in the delay caused that the spikes were fired even earlier than the peaks of the oscillatory current (Fig. 5G, H; vertical dotted line indicates the peak of oscillatory current used as the reference 0 deg). This reduction in the phase-shift is traduced into an average phase advance in spiking in 22, 18 and 13 deg for 4, 6 and 8 Hz, respectively (Fig. 5I, top trace). In the time domain, this manipulation gives average advances in spike timing of 15.4, 8.4 and 4.6 ms for 4, 6 and 8 Hz, respectively (Fig. 5I, bottom trace). These results support the notion that the modulation of Φ at subthreshold potentials is also manifested in the evoked resonance.

DISCUSSION

The main interest behind resonance is its coincident frequency range with the theta activity observed in most brain regions during behavior (Colgin, 2013). This suggests the possibility that individual neurons are endowed with a mechanism of frequency selectivity, which could allow them to be engaged during behaviorally relevant theta activity (Hutcheon and Yarom, 2000; Izhikevich, 2002; Lisman and Jensen, 2013; Schmidt et al., 2017; but see Stark et al., 2013). Resonant neurons from different brain regions display diverse frequency selectivity along the theta band, suggesting different functional specializations. Moreover, the modulation of resonance resulting from the interaction of neuronal intrinsic factors and external influences could allow the dynamical entrainment of groups of cells during changing network oscillatory states.

Here we characterized the natural diversity of subthreshold I_h-dependent resonance in three known types of cortical neurons, assessed the dynamic modulation of subthreshold resonance in individual cells by modifying specific neuronal properties and evaluated whether these regulatory processes could influence spiking probability and timing. We found that the distribution of the f_R values from the whole population of theta-resonant cells follows a continuous, negative power-law relationship with R_{in} along the theta range. The f_R values from each group are distributed in subranges within the theta frequencies, displaying some degree of overlapping. We also showed that neurons that undergo fluctuations in R_{in} as a consequence of changes in holding potential or total somatic conductance mimicking modifications in passive or synaptic currents, display a change in f_R that follows the same rule. Importantly, we demonstrated that this modulation of f_R can effectively influence the selective firing of cortical neurons at theta frequencies, modifying the output frequency in ~2 Hz.

Considering the diverse structural and electrophysiological features of the studied cell types and the published results about their average frequency selectivity, it was expected that they would display different resonance properties. However, testing their behavior in the same experimental conditions allowed a more detailed comparison of the resonant behavior of heterogeneous populations of neurons. At hyperpolarized potentials, we found clear differences in the f_R average values for each group along the theta band, as well as in other resonance features. f_R was higher in SL than in HP and reached its lowest value in AM. We also observed variability in the resonant behavior in cells of the same type. Diverse factors could underlie these differences, such as dissimilar properties and distribution of voltage-dependent conductances, differences in the passive membrane properties, cell size and morphology.

Differences in I_h-dependent frequency preference have been reported in distinct brain regions, among locations of the same structure, as well as along the somato-dendritic axis of individual neurons. SL neurons display a gradient in f_R along the dorso-ventral axis of the entorhinal cortex, caused by differences in the properties of the HCN-channels (Giocomo and Hasselmo, 2008); larger I_h time constants in the ventral region generate lower f_R. Interestingly, the f_R gradient along the dorso-ventral axis is accompanied by opposite changes in R_{in} and intrinsic cell excitability. Moreover, a higher HCN-channel and *h*-current densities at the distal dendritic region of CA1 pyramidal cells increase f_R and Φ_p along the somato-dendritic axis (Magee, 1998; Narayanan and Johnston, 2007, 2008). This spatial gradient in I_h also generates opposed differences in R_{in} and a corresponding modification in cell excitability along dendrites (Magee, 1998; Narayanan and Johnston, 2007). On the other hand, the induction of NMDAR-dependent long-term synaptic potentiation or depression generates an increase or decrease in f_R, respectively, along the somato-dendritic axis of CA1 pyramidal neurons, relying on opposed changes in *h* conductance (Brager and Johnston, 2007; Narayanan and Johnston, 2007). Hebbian synaptic plasticity also causes compensatory modifications in R_{in} and neuron excitability that inversely correlate with f_R changes. Moreover, up or down regulation of I_h-maximal conductance underlies homeostatic changes in excitability after chronic activity enhancement or deprivation in CA1 pyramidal neurons (Gasselin et al., 2015). These observations are in line with the inverse correlation between f_R and R_{in} that we are reporting. Moreover, we found an empirical rule describing this relationship that holds for the whole population of neurons, in spite of the strong heterogeneity of the different groups.

An interesting point that emerges from the relationship between R_{in} and f_R is that the range of R_{in} naturally occurring in neurons, sets and constrains the frequency preference specifically to the theta range, mostly between 2 and 10 Hz. Moreover, in subsequent experiments we show that, while the R_{in} of SL neurons ranges from 10 to 50 MΩ at rest, it can reach up to 100 MΩ at perithreshold conditions, with f_R fluctuating within the theta range. A similar interval of modulation was obtained for constant conductance injections that change R_{in} in a physiological range.

To explore the basis of this relationship and how it depends on the properties of the different cells, we compared the results with those predicted by the analysis of linear systems (Richardson et al, 2003; Rotstein and Nadim, 2014; for more details, see the Appendix). While this formalism was developed for spherical (or point) cells and makes additional assumptions, it provides a first approximation to explore trends relating neuronal properties and resonance attributes. For hyperpolarized membrane potentials, we only considered I_h and I_{Leak}. Using R_{in} and the measured resonance and phase attributes, we obtained numerical estimations of the membrane parameters underlying the differential frequency selectivity of our cells. The exploration pointed to differences in the densities of the HCN channels or a stronger coupling among I_h and voltage, as the basis for resonance diversity among the different neuron types. No apparent influence of the passive membrane conductance was detected in the case of SL and HP. A similar interpretation stands for to the variability inside a group (only HP cells were compared to each other). In the case of AM neurons, additional influences of passive properties may exist.

Changes in R_{in} would modify the excitability of neurons, as observed along the dorso-ventral axis of the entorhinal cortex and along the dendrites of hippocampal cells (see above). A simple explanation is the presence of diverse I_h properties, including differences in HCN density and distribution, as well as in voltage- and time-dependent activation. While in our case the f_R-R_{in} relationship holds for the somato-dendritic compartment of neurons, these previous results suggest that it may be a more general property. Whether these observations can be generalized to other forms of subthreshold resonance or to other cell types like resonant GABAergic interneurons, requires to be determined.

Differences in passive membrane properties and cytoarchitecture should also be considered. In fact, in contrast to the predictions for SL and HP neurons, the resonant behavior of AM neurons suggested differences in the passive properties. Among them can be the expression levels of background conductances like GIRK or two-pore domain K^+ channels (Enyedi and Czirjak, 2010; Kim and Johnston, 2015) and the total membrane area and shape of the somato-dendritic compartment. While there is no available information about heterogeneities in the expression of background conductances in the studied neurons, there is a clear difference in the size of the cell bodies and main dendrites that conform their somato-dendritic compartment. AM neurons are the smallest, with spherical ∼10 μm somas and relatively short dendrites, HP neurons have pyramidal 15–20 μm somas and SL neurons have a multipolar shape with a soma of ∼23 μm and multiple dendrites highly branched producing the stellate shape (Klink and Alonso, 1997). This diversity is expected to influence ionic fluxes among cellular compartments and spatiotemporal signal integration, with an impact in both R_{in} and f_R values in different cell locations.

Among the factors that influence R_{in} and can contribute to the dynamic modulation of f_R and Φ are the activation levels of subthreshold voltage-sensitive conductances. When cortical neurons depolarize, R_{in} varies due to activation or deactivation of voltage-dependent conductances like G_h, G_M or G_{NaP} (Surges et al., 2004; Yamada-Hanff & Bean, 2015; Ceballos et al., 2017; Vera et al., 2017), resulting in nonlinear amplification of voltage responses when tested outside of the linear regime (Rotstein, 2015). We showed that, by using low amplitude stimuli causing a voltage deflection around 5 mV peak-to-peak and generating a quasi-linear cellular response, resonance varies according to fluctuations of R_{in}, following the f_R-R_{in} rule. At hyperpolarized potentials, I_h reaches a maximum and R_{in} a minimum (Surges et al., 2004). At this point, the neurons express their highest f_R and lowest Φ (fastest response). At more depolarized potentials (above −70 mV) the decrease in I_h is expected to moderately increase R_{in} and Z_{Max}, shifting f_R to lower values and increasing Φ. However, above −70 mV, I_{NaP} starts to activate, favoring a further increase in R_{in} (Ceballos et al., 2017; Vera et al., 2017). Thus, the currents that increase the impedance and amplify resonance (like I_{NaP}) might play a pivotal role in the tuning of the frequency preference and neuron response timing, raising the perithreshold R_{in}, increasing the range for f_R and Φ modulation and facilitating the communication of resonance to the spiking regime.

One limitation of our experimental approach is that we focused our manipulation to constrain neural responses inside a quasi-linear range, by applying low amplitude of ZAP stimuli. In this regime, we minimized the contribution of nonlinearities that might arise from the interaction between resonant and amplifying voltage-dependent currents, as predicted by mathematical models (Rotstein, 2015). In SL and AM neurons, perithreshold resonance depends on I_h and if high enough levels of I_{NaP} are recruited, nonlinear amplifications can occur. Further experimental investigation is required to understand the effects of nonlinearities in the modulation of subthreshold resonant behavior and input resistance of heterogeneous populations of neurons, as well as in the tuning of firing behavior.

In addition to R_{in} changes resulting from modifications of the leak or voltage-dependent conductances, a major source of R_{in} variation is the activation of synaptic receptors. Regardless of their excitatory or inhibitory nature, their activation by synaptic stimulation increases the membrane conductance with a consequent reduction in R_{in}. It has been postulated that neurons that are part of active circuits *in vivo* receive a plethora

of uncorrelated excitatory and inhibitory synaptic inputs that generates drastic R_{in} variations, as a drop to 10% of the values observed *in vitro* (reviewed in Destexhe et al., 2003). According to our results, controlled conductance increases rises f_R in ~2 Hz. Therefore, we can hypothesize that massive conductance fluctuations, as those due to dynamic changes in synaptic bombardment, could allow a fast tuning of f_R. These results agree with previous theoretical work that proposed changes in membrane conductance as a mechanism to modulate resonance (Hutcheon et al., 1996a; Richardson et al., 2003; Rotstein and Nadim, 2014). Our experimental results and computer simulations allow estimating the range of f_R and R_{in} modifications that could occur during conductance changes produced by variations in synaptic tone in natural conditions and provide a framework to structure this modulation by dynamically moving on the f_R-R_{in} curve along the theta range. Interestingly, recent work showed that human cortical neurons display a high R_{in} at the dendrites due to a reduction in the number of ion channels (Beaulieu-Laroche et al., 2018), raising the possibility of a large range of resonance modulation in human neurons.

In order to have a role in neuronal processing, subthreshold resonance should influence action potential firing. The relationship between subthreshold resonance and evoked firing is complex and not completely understood (Rotstein, 2017a). For low enough input amplitudes, resonant neurons could communicate their subthreshold frequency selectivity to the firing regime, as has been observed *in vitro* and in theoretical works (Pape et al., 1998; Pape and Driesang, 1998; Erchova et al., 2004; Ulrich, 2002; Vera et al., 2014, 2017; Rotstein, 2017a), and also *in vivo* under anesthesia (Kamondi et al., 1998; but see Stark et al., 2013). For a cell depolarized to a voltage close to action potential threshold, it is more probable that subthreshold resonance could influence the firing frequency. In behaving animals, intracellular recordings in both SL and HP neurons showed that, when coding space (grid or space field, respectively), neurons are depolarized to perithreshold level, the membrane potential oscillates at theta frequency and they fire at the peak of the oscillations (Harvey et al., 2009; Domnisoru et al., 2013). While it is not clear whether these neuronal theta oscillations result from resonant filtering of synaptic inputs or correspond to intrinsic subthreshold membrane potential oscillations, there is a large body of evidence showing that cells receive theta oscillatory inputs generated by the coordinated activity from multiple theta oscillators of the septum, as well as by oscillatory activity generated inside the hippocampal region (reviewed in Colgin, 2013). Therefore, it could be hypothesized that, under physiological conditions, resonant neurons receive theta oscillatory inputs that can be selectively filtered by resonance. We showed that the firing probability of a neuron is regulated by adding or subtracting a virtual constant somatic conductance. In a neuron displaying resonance at perithreshold potentials, a slight increment in the steady-state depolarization or stimulus amplitude would lead the cell to fire with a higher probability at f_R. In this speculative scenario, a constant synaptic tone or the average steady-state component of a synaptic noise (Rudolph et al., 2004), could be the external variables depolarizing the neuron beyond threshold, modulating the frequency preference along the theta band and adjusting the timing of spikes in the millisecond range. While the increase in conductance is expected to reduce cell excitability, we have shown that this does not preclude the emergence of spiking resonance, probably because of the high R_{in} values attained at perithreshold potentials. The extent at which the proposed model holds under physiological conditions remains to be addressed.

In summary, we provide detailed evidence for the natural variability of f_R and Φ among different cell types and in each cell type. Despite the high heterogeneity in the resonant properties, the f_R and Φ of cortical neurons can be set along the theta range in a close inverse relationship to their R_{in}. It is noteworthy that, in spite of all the factors that could influence resonance and R_{in} (like the magnitude and distribution of membrane conductances, dendritic and somatic morphologies, etc.), it is still possible to find such a high degree of correlation among them. Moreover, during changes in individual cells like increases in the overall conductance or depolarization to perithreshold levels, the f_R-R_{in} is preserved. This suggests that these variables are linked in more general terms, that could be related to neuron excitability. Importantly, as subthreshold and evoked spiking resonance can be regulated by changes that may occur under physiological conditions, the frequency preference could be dynamically adjusted. Whether cortical circuits effectively implement this mechanism of f_R modulation to promote changes in the oscillatory activity along the theta range requires further investigation.

ACKNOWLEDGMENTS

We thank Pablo Villar for helpful discussions and Dr. Alain Marty for thoughtful comments on previous versions of the manuscript. This work was funded by the Chilean Fund for Scientific and Technological Development (FONDECYT) regular grants 1140700 (MS) and 1140520 (JB), and the postdoctoral grant 3150668 (JV).

REFERENCES

Beaulieu-Laroche L, Toloza EHS, van der Goes MS, Lafourcade M, Barnagian D, Williams ZM, Eskandar EN, Frosch MP, Cash SS, Harnett MT (2018) Enhanced dendritic compartmentalization in human cortical neurons. Cell 175:643–651.e14.

Biel M, Wahl-schott C, Michalakis S, Zong X (2009) Hyperpolarization-activated cation channels: from genes to function. Physiol Rev 89:847–885.

Brager DH, Johnston D (2007) Plasticity of intrinsic excitability during long-term depression is mediated through mGluR-dependent changes in Ih in hippocampal CA1 pyramidal neurons. J Neurosci 27:13926–13937.

Buzsáki G (2006) Rhythms of the brain. USA: Oxford University Press.

Ceballos CC, Roque AC, Lea RM (2017) A negative slope conductance of the persistent sodium current prolongs subthreshold depolarizations. Biophys J 113:2207–2217.

Colgin LL (2013) Mechanisms and functions of theta rhythms. Annu Rev Neurosci 36:295–312.

Contreras D (2004) Electrophysiological classes of neocortical neurons. Neural Netw 17:633–646.
Destexhe A, Rudolph M, Pare D (2003) The high-conductance state of neocortical neurons in vivo. Nat Rev Neurosci 4:739–751.
Domnisoru C, Kinkhabwala A, Tank DW (2013) Membrane potential dynamics of grid cells. Nature 495:199–204.
Dorval AD, Christini DJ, White JA (2001) Real-time Linux dynamic clamp: a fast and flexible way to construct virtual ion channels in living cells. Ann Biomed Eng 29:897–907v.
Economo MN, Martínez JJ, White JA (2014) Membrane potential-dependent integration of synaptic inputs in entorhinal stellate neurons. Hippocampus 13:1–13.
Enyedi P, Czirjak G (2010) Molecular background of leak K currents: two-pore domain potassium channels. Physiol Rev 90:559–605.
Erchova I, Kreck G, Heinemann U, Herz AM (2004) Dynamics of rat entorhinal cortex layer II and III cells: characteristics of membrane potential resonance at rest predict oscillation properties near threshold. J Physiol 560:8910.
French CR, Sah P, Buckett KJ, Gage PW (1990) A voltage-dependent persistent sodium current in mammalian hippocampal neurons. J Gen Physiol 95:1139–1157.
Gasselin C, Inglebert Y, Debanne D (2015) Homeostatic regulation of h-conductance controls intrinsic excitability and stabilizes the threshold for synaptic modification in CA1 neurons. J Physiol 593:4855–4869.
Giocomo LM, Hasselmo ME (2008) Time constants of h current in layer ii stellate cells differ along the dorsal to ventral axis of medial entorhinal cortex. J Neurosci 28:9414–9425.
Giocomo LM, Zilli EA, Fransén E, Hasselmo ME (2007) Temporal frequency of subthreshold oscillations scales with entorhinal ggrid cell field spacing. Science 315:1719–1722.
Golowasch J, Thomas G, Taylor AL, Patel A, Pineda A, Khalil C, Nadim F (2009) Membrane capacitance measurements revisited: dependence of capacitance value on measurement method in nonisopotential neurons. J Neurophysiol 102:2161–2175.
Gutfreund Y, Yarom Y, Segev I (1995) Subthreshold oscillations and resonant frequency in guinea-pig cortical neurons: physiology and modelling. J Physiol 483(3):621–640.
Harvey CD, Collman F, Dombeck DA, Tank DW (2009) Intracellular dynamics of hippocampal place cells during virtual navigation. Nature 461:941–946.
Hodgkin AL, Huxley AF (1952) A quantitative description of membrane current and its application to conduction and excitation in nerve. J Physiol 117:500–544.
Hu H, Vervaeke K, Storm JF (2002) Two forms of electrical resonance at theta frequencies, generated by M-current, h-current and persistent Na $^{+}$ current in rat hippocampal pyramidal cells. J Physiol 545:783–805.
Hu R, Whiteus CB, Meijer DH, Ferguson KA, Araneda RC (2016) Hyperpolarization-activated currents in granule cells of the olfactory bulb. eNeuro 009817:9817.
Hutcheon B, Miura RM, Puil E (1996a) Models of subthreshold membrane resonance in neocortical neurons. J Neurophysiol 76:698–714.
Hutcheon B, Miura RM, Puil E (1996b) Subthreshold membrane resonance in neocortical neurons. J Neurophysiol. 76 (2):683–697. https://doi.org/10.1152/jn.1996.76.2.683.
Hutcheon B, Yarom Y (2000) Resonance, oscillation and the intrinsic frequency preferences of neurons. Trends Neurosci 23:216–222.
Izhikevich EM (2002) Resonance and selective communication via bursts in neurons having subthreshold oscillations. Biosystems 67:95–102.
Kaczorowski CC, Disterhoft J, Spruston N (2011) Stability and plasticity of intrinsic membrane properties in hippocampal CA1 pyramidal neurons: effects of internal anions. J Physiol 3:799–818.
Kamondi A, Acsady L, Wang X-J, Buzsáki G (1998) Theta oscillations in somata and dendrites of hippocampal pyramidal cells in vivo: activity-dependent phase-precession of action potentials. Hippocampus 261:244–261.
Kass R, Eden U, Brown E (2014) Analysis of neural data. New York: Springer.
Kay LM (2005) Theta oscillations and sensorimotor performance. Proc Natl Acad Sci U S A 102:3863–3868.
Kim CS, Johnston D (2015) A1 adenosine receptor-mediated GIRK channels contribute to the resting conductance of CA1 neurons in the dorsal hippocampus. J Neurophysiol. 113(7):2511–2523. https://doi.org/10.1152/jn.00951.2014. Epub 2015 Feb 4PMID: 25652929.
Klink R, Alonso A (1997) Morphological characteristics of layer II projection neurons in the rat medial entorhinal cortex. Hippocampus 7:571–583.
Lisman J, Buzsáki G (2008) A neural coding scheme formed by the combined function of gamma and theta oscillations. Schizophr Bull 34:974–980.
Lisman JE, Jensen O (2013) The theta-gamma neural code. Neuron 77:1002–1016.
Lopes-dos-Santos V, van de Ven GM, Morley A, Trouche S, Campo-Urriza N, Dupret D (2018) Parsing hippocampal theta oscillations by nested spectral components during spatial exploration and memory-guided behavior. Neuron 100:940–952.
Magee JC (1998) Dendritic hyperpolarization-activated currents modify the integrative properties of hippocampal CA1 pyramidal neurons. J Neurosci 18:7613–7624.
Mizuseki K, Sirota A, Pastalkova E, Buzsáki G (2009) Theta oscillations provide temporal windows for local circuit computation in the entorhinal-hippocampal loop. Neuron 64:267–280.
Narayanan R, Johnston D (2007) Long-term potentiation in rat hippocampal neurons is accompanied by spatially widespread changes in intrinsic oscillatory dynamics and excitability. Neuron 56:1061–1075.
Narayanan R, Johnston D (2008) The h channel mediates location dependence and plasticity of intrinsic phase response in rat hippocampal neurons. J Neurosci 28:5846–5860.
Neher E (1992) Correction for liquid junction potentials in patch clamp experiments. Methods Enzymol 207:123–131.
Pape H, Paré D, Driesang RB (1998) Two types of intrinsic oscillations in neurons of the lateral and basolateral nuclei of the amygdala. J Neurophysiol 1:205–216.
Pape HC, Driesang RB (1998) Ionic mechanisms of intrinsic oscillations in neurons of the basolateral amygdaloid complex. J Neurophysiol 79:217–226.
Peters HC, Hu H, Pongs O, Storm JF, Isbrandt D (2005) Conditional transgenic suppression of M channels in mouse brain reveals functions in neuronal excitability, resonance and behavior. Nat Neurosci 8:51–60.
Puil E, Gimbarzevsky B, Miura RM (1986) Quantification of membrane properties of trigeminal root ganglion neurons in guinea pigs. J Neurophysiol 55:995–1016.
Puil E, Meiri H, Yarom Y (1994) Resonant behavior and frequency preferences of thalamic neurons. J Neurophysiol 71:575–582.
Ranade S, Hangya B, Kepecs A (2013) Multiple modes of phase locking between sniffing and whisking during active exploration. J Neurosci 33:8250–8256.
Richardson MJE, Brunel N, Hakim V (2003) From subthreshold to firing-rate resonance. J Neurophysiol 89:2538–2554.
Rotstein HG (2014) Frequency preference response to oscillatory inputs in two-dimensional neural models: a geometric approach to subthreshold amplitude and phase resonance. J Math Neurosci 4:11.
Rotstein HG (2015) Subthreshold amplitude and phase resonance in models of quadratic type: nonlinear effects generated by the interplay of resonant and amplifying currents. J Comp Neurosci 38:325–354.
Rotstein HG (2017a) Spiking resonances in models with the same slow resonant and fast amplifying currents but different subthreshold dynamic properties. J Comp Neurosci 43:243–271.
Rotstein HG (2017b) The shaping of intrinsic membrane potential oscillations: positive/negative feedback, ionic resonance/amplification, nonlinearities and time scales. J Comp Neurosci 42:133–166.

Rotstein HG, Nadim F (2014) Frequency preference in two-dimensional neural models: a linear analysis of the interaction between resonant and amplifying currents. J Comput Neurosci 37:9–28.
Rudolph M, Piwkowska Z, Badoual M, Bal T, Destexhe A (2004) A method to estimate synaptic conductances from membrane potential fluctuations. J Neurophysiol 91:2884–2896.
Sanhueza M, Bacigalupo J (2005) Intrinsic subthreshold oscillations of the membrane potential in pyramidal neurons of the olfactory amygdala. Eur J Neurosci 22:1618–1626.
Schmidt SL, Dorsett CR, Iyengar AKFF (2017) Interaction of intrinsic and synaptic currents mediate network resonance driven by layer V pyramidal cells. Cereb Cortex 1:4396–4410.
Spain WJ, Schwindt PC, Crill WE (1987) Anomalous rectification in neurons from cat sensorimotor cortex in vitro. J Neurophysiol 57:1555–1576.
Spruston N, Johnston D (1992) Perforated patch-clamp analysis of the passive membrane properties of three classes of hippocampal neurons. J Neurophysiol 67:508–529.
Stark E, Eichler R, Roux L, Fujisawa S, Rotstein HG, Buzsáki G (2013) Inhibition-Induced theta resonance in cortical circuits. Neuron 80:1263–1276.
Surges R, Freiman TM, Feuerstein TJ (2004) Input resistance is voltage dependent due to activation of I h channels in rat CA1 pyramidal cells. J Neuro Res 76:475–480.
Ulrich D (2002) Dendritic resonance in rat neocortical pyramidal cells. J Neurophysiol 87:2753–2759.
Vera J, Alcayaga J, Sanhueza M (2017) Competition between persistent Na+ and muscarine-sensitive K+ currents shapes perithreshold resonance and spike tuning in CA1 pyramidal neurons. Front Cell Neurosci 11:61. https://doi.org/10.3389/fncel.2017.00061.
Vera J, Pezzoli M, Pereira U, Bacigalupo J, Sanhueza M (2014) Electrical resonance in the θ frequency range in olfactory amygdala neurons. PLoS One 9 e85826.
Wilson MA, Varela C, Remondes M (2015) Phase organization of network computations. Curr Opin Neurobiol 31:250–253.
Xu J, Kang N, Jiang L, Nedergaard M, Kang J (2005) Activity-dependent long-term potentiation of intrinsic excitability in hippocampal CA1 pyramidal neurons. J Neurosci 25:1750–1760.
Yamada-hanff J, Bean BP (2015) Activation of Ih and TTX-sensitive sodium current at subthreshold voltages during CA1 pyramidal neuron firing. J Neurop 114:2376–2389.

APPENDIX

Parameter exploration for a linear system

We have assessed the natural variability of subthreshold frequency preference among heterogeneous populations of theta-resonant neurons and evaluated the changes produced by controlled modifications in G_{Leak} or by adjusting the holding potential.

Along our experiments, we studied the linear resonant behavior of our neurons by applying low enough input currents. Linearized conductance-based models have been used to characterize resonance in terms of the properties of the involved membrane currents (Richardson et al., 2003; Rotstein and Nadim, 2014). This formalism provides a simplified framework for modelling systems with different resonant and amplifying currents. The three cell types we are studying display I_h-dependent resonance at hyperpolarized membrane potentials, and thus a minimal model should comprise I_h and I_{Leak}. These studies addressed the modifications in resonance attributes occurring after changes in one or a combination of the neuronal biophysical parameters and membrane potential (Richardson et al., 2003; Rotstein and Nadim, 2014). Moreover, the impedance and phase profiles can be calculated analytically. Therefore, comparing our experimental results with the predictions of these models can provide hints about the membrane features that may underlie the resonance heterogeneity of our cells along the theta band. This approach could also predict the changes in resonance parameters observed upon different experimental manipulations, as well as their relationship to R_{in}.

We first aimed to explore the factors that could influence the diverse resonant behavior of the three cell types. Interestingly, in spite of the diversity in size, morphology and other electrophysiological properties of the neurons from the three regions, we were able to detect some trends by using a linear spherical model. This model applies for small voltage fluctuations around a fixed holding voltage $\overline{V}$. In this approximation, theoretical equations for the impedance and phase profiles, $Z(f)$ and $\Phi(f)$, respectively, can be derived and expressed in terms of four parameters: the cell capacitance C, the I_h activation time constant τ_h and the *effective leak* and *ionic conductances*, g_L and g_1, evaluated at $\overline{V}$ (Richardson et al., 2003; Rotstein and Nadim, 2014). Note that g_1 represents the coupling between voltage and I_h.

$$g_L = G_{Leak} + G_h X_{1,\infty}(\overline{V}) \tag{10}$$

$$g_1 = G_h X'_{1,\infty}(\overline{V})(\overline{V} - E_h), \tag{11}$$

G_{Leak} and G_h are the maximal biophysical conductances (in nS) for I_{Leak} and I_h, and $X_{1,\infty}$ is the steady-state activation curve for I_h. A detailed investigation of the dependencies of the $Z(f)$ and $\Phi(f)$ profiles on these parameters was conducted in (Rotstein and Nadim, 2014). We will use these tools to discuss our observations and explore the intrinsic factors that may contribute to the diversity in the resonance properties of our cells. For this, it is useful to define the biophysical conductance densities G_{Leak}^* and G_h^* (where $Gi^* = Gi/C$, in nS/pF) and the effective conductance densities g_L^* and g_1^* ($g_i^* = g_i/C$, nS/pF).

In both theoretical and experimental studies, the mostly used parameters to characterize $Z(f)$, are f_R, Z_{Max}, the resonance strength Q and the frequency selectivity (impedance right-bandwidth). An alternative approach is to consider R_{in} as an experimental measure of the zero-frequency impedance $Z(0)$.

The analytical expressions for f_R, the zero-phase (phasonant) frequency f_P and Z_{Max} (Richardson et al., 2003; Rotstein and Nadim, 2014), are

$$f_R = \frac{1}{2\pi\tau_h}\left\{\left[\left(\tau_h(g_L^* + g_1^*) + 1\right)^2 + \left(\tau_h g_L^* + 1\right)^2\right]^{1/2} - 1\right\}^{1/2} \tag{12}$$

$$f_p = \frac{1}{2\pi\tau_h}\left[\tau_h g_1^* - 1\right]^{1/2} \tag{13}$$

$$Z_{Max} = \frac{\tau_h}{C}\left\{\frac{1 + (2\pi f_R \tau_h)^2}{\left(\tau_h(g_L^* + g_1^*) - (2\pi f_R \tau_h)^2\right)^2 + (2\pi f_R \tau_h)^2(1 + \tau_h g_L^*)^2}\right\}^{1/2} \tag{14}$$

In addition, analytical expression for R_{in} can be obtained by applying the linear approximation for a low-amplitude current step,

$$R_{in} = \frac{1}{c(g_L^* + g_1^*)} \quad (15)$$

In our case, we obtained experimentally the values of these resonance attributes and explored the differences in membrane properties that could contribute to the observed heterogeneity. We will first summarize some general trends outlining the influence of the different membrane parameters on Z and Φ profiles (Rotstein and Nadim, 2014). A first factor to be considered while analyzing cell diversity are the differences in membrane capacitance (see Table 1 for estimated average values of C for each population). In the trivial case in which the cells from the different groups displayed similar G_{Leak}^* and G_h^*, and I_h time and voltage-dependencies, i.e. for preserved τ_h, g_L^* and g_1^*, an increase in C would cause the whole impedance curve to decrease by a factor, with $Z_1(f)/Z_2(f) = C_2/C_1$. Thus, C differences may strongly and inversely affect both Z_{Max} and R_{in}. On the other hand, f_R, Q and the whole Φ profile are independent of C. With respect to the time constant τ_h, it influences Z in the theta band, but it is less relevant for lower or higher frequencies. As is the case for Z at 20 Hz and for R_{in} (Z(0)). For fixed values of g_L^* or g_1^*, an increment in τ_h reduces the filtering effect of I_h and thus is expected to increase Z_{Max} and Q(Z(0) does not change). On the other hand, increases in τ_h should reduce both f_R and f_P. With regards to the effective conductances, increases in either g_L^* or g_1^* should increment f_R and reduce R_{in} and Z_{Max}. However, g_1^* increases Q (because R_{in} decreases more than Z_{Max}), while g_L^* decreases it. It should be noted, however, that modifications in g_1^* or g_L^* could be due to differences in the biophysical conductances or in the I_h steady-state activation curve, or both. In the linear approach, resonance is described in terms of the effective conductances and thus it is not possible to dissect which are the biophysical bases of the differences in g_1^*, unless the voltage-dependence of I_h in each specific cell species were known (Eq. (11)). Note also that changes in g_1^* will in general be accompanied by modifications in g_L^* (Eqs. (10) and (11)). On the other hand, changes in g_L^* would also be accompanied by modifications in g_1^*, with the exception of changes involving G_{Leak}^* only. Therefore, in general, it is not straightforward to predict the impact of changes in the effective conductances separately. However, some observations could provide hints in specific cases. Increases in G_{Leak}^* should decrease the whole Z curve, thus, while I_h does not affect the magnitude of Z at high frequencies, changes in G_{Leak}^* do. Hence, comparing $Z(20)$ among cells after correcting for the differences in C, allows detecting possible changes in G_{Leak}^*. Also, while an increment in either G_h^* or G_{Leak}^* would increase f_R and decrease Z_{Max} and R_{in}, a critical difference is that G_h^* would rise and G_{Leak}^* diminish the resonance strength Q.

As several intrinsic parameters could vary among the three heterogeneous populations of resonant cells, the exploration of the factors influencing resonance heterogeneity is expected to be complex and the conclusions may be limited. A simpler situation to explore the application of these concepts are the experiments from Fig. 3, where a change in G_{Leak}^* was mimicked in HP cells by adding or subtracting a virtual constant conductance G through the dynamic clamp, while keeping constant the steady-state voltage $\overline{V}$. As expected, in the $G > 0$ condition (higher G_{Leak}^*), f_R increases while Z_{Max}, R_{in} and Q decrease relative to control (Fig. 3F–H). Note also that a decrease in Z at 20 Hz is observed in Fig. 3E (left), even though in these experiments the average C is not changing, which is consistent with the experimentally generated increase in G_{Leak}^*. Finally, in line with the constant G_h^* in these experiments, f_P does not change significantly (Fig. 3J and Eq. 13). The opposite occurs for $G < 0$. Thus, in these experiments the trends for the changes in Z and Φ are those expected for increasing or decreasing the G_{Leak}^*, while keeping unaltered the other membrane parameters and $\overline{V}$.

We will first examine resonant behavior in HP and SL neurons (HP-SL direction). The increase in C among these cells would cause by itself a reduction in Z by a factor of $Z_{SL}/Z_{HP} = C_{HP}/C_{SL} \sim 0.75$ (see Table 1). However, the observed decrease in Z_{Max} and R_{in} were higher, with $Z_{Max,SL}/Z_{Max,HP} = 0.61$ and $R_{in,SL}/R_{in,HP} = 0.4$. Possible explanations are increases in either g_1^*, relying on a higher G_h^* or a stronger coupling between voltage and I_h, expressed by the steepness of the activation curve, or in g_L^*, as well as decreases in τ_h (only for Z_{Max}, as R_{in} is measured at steady-state conditions and is independent of τ_h). Similar changes in parameters (higher g_1^* or g_L^*, or lower τ_h) could underlie the higher f_R in SL (8.7 Hz) compared to HP (6.5 Hz). Moreover, zero-phase frequency f_P is also higher in SL (HP: 2.9 ± 0.24 Hz, $n = 11$; SL: 6.05 ± 0.27 Hz, $n = 11$; $T = 8.6$, $P = 3.8$ E-8). In contrast to f_R, f_P only depends on g_1^* and τ_h, in opposite ways: while g_1^* increases f_P, τ_h decreases it. Thus, the higher f_P in SL would result from the balance between these two parameters. On the other hand, the increase in Q in the HP-SL direction ($Q_{HP} = 1.23$, $Q_{SL} = 1.62$; Table 2) is also consistent with a higher g_1^*. In contrast, a higher g_L^* or a lower τ_h would have the opposite effect on Q. Interestingly, when comparing the values of $Z(20)$, (that depends on C and G_{Leak}^*), we found that $Z(20)_{,SL}/Z(20)_{,HP} \sim 0.7$, supporting a major influence of C, as $C_{HP}/C_{SL} \sim 0.75$). This suggests that the biophysical conductance density G_{Leak}^* does not significantly differ in these two cell types. Overall, our observations suggest that, at −80 mV, the differences in resonance properties of HP and SL neurons mainly rely on a higher G_h^* or I_h activation level in the second group. It is not clear a priori which could be the differences in τ_h, as some observations suggest it may be higher in SL and others, the opposite. Finally, the similar values of Z at 20 Hz in SL and HP neurons, after correcting for C, suggest that both cell types may have comparable G_{Leak}^* values.

We will later use a quantitative approach to estimate the values of the parameters, based on the analytical

Table 4. τ_h, g_1* and g_L* parameters calculated from a linearized conductance-based model of resonance, using the experimental values of R_{in}, Z_{Max} f_R and f_P. C values were estimated from the experiments. The biophysical conductances G_h* and G_{Leak}* were calculated using published I_h steady-state activation functions for of SL and HP cells (see Text). The SL function was used for AM cells

	C (pF)	τ_h (ms)	g_L* (nS/pF)	g_1* (nS/pF)	Gh* (nS/pF)	G_L* (nS/pF)
SL	160	66	0.125	0.109	0.107	0.07
HP	120	43	0.095	0.033	0.035	0.085
AM	80	38	0.044	0.017	0.019	0.035

equations for the Z and Φ profiles (Richardson et al., 2003; Rotstein and Nadim, 2014) and using general available information about the I_h voltage-dependence and kinetics in SL and HP cells.

When considering the differences in the AM-HP direction, similar trends as for HP-SL were observed in most, but not all, resonance attributes. Shared features were an increase in f_R, a decrease in Z_{Max} (beyond the expected reduction due to the higher C in HP) and a rise in Q (see details in Table 2), also supporting an increase in g_1* in the AM-HP direction. However, the differences in the whole impedance curve were significantly more pronounced than for HP-SL. The comparison of Z at 20 Hz in the AM-HP direction showed a reduction of $Z_{HP(20)}/Z_{AM(20)} \sim 0.45$, which cannot be fully explained by the increase in C, as $C_{AM}/C_{HP} \sim 0.67$. This suggests that, besides the increase in g_1* between AM and HP, an additional increase in G_{Leak}* could occur. When comparing f_P among these populations, a trend was observed for a lower value in AM, however, the differences were not statistically significant (AM: 1.83 ± 0.45 Hz, $n = 7$; HP: 2.9 ± 0.24 Hz, $n = 11$; $T = 2.1$, $P = 0.07$), perhaps due to the more noisy Φ curve at low frequencies.

For a closer exploration of the intrinsic properties influencing resonance in the three cell types, we used the analytical expressions for $Z(f)$ and $\Phi(f)$ derived using the linear system approximation (Richardson et al., 2003; Rotstein and Nadim, 2014). By solving these equations for τ_h, g_1* and g_L* in terms of R_{in} and other measured resonance attributes as f_R, Z_{Max} and f_p (Table 2), we obtained numerical estimations of these parameters (we used the approximated average C values displayed in Table 1). Interestingly, combining the Eqs. (12), (14) and (15), expressed in terms of the effective conductance densities, we obtained the following equation for the time constant τ_h:

$$\tau_h = \frac{1}{(2\pi f_R)^2 C}\left[\left(\frac{1}{R_{in}}\right)^2 - \left(\frac{1}{Z_{Max}}\right)^2\right]^{1/2} \quad (16)$$

The C values used and the calculated τ_h were, SL: $C = 160$ pF, $\tau_h = 66$ ms; HP: $C = 160$ pF, $\tau_h = 43$ ms and AM: $C = 160$ pF, $\tau_h = 66$ ms. Notably, the reported τ_h for SL and HP around −80 mV are ∼73 ms and ∼47 ms, respectively, in close agreement with the calculated values (Magee, 1998; Giocomo and Hasselmo, 2008).

Next, we obtained g_1* from Eq. (13), and g_L* from Eq. (15), introducing the average experimental values of f_P and R_{in}. In the case of SL and HP cells, we used published values for the steady-state activation curves of I_h ($V_{1/2} = -79$ mV, $k = 9.8$, for SL and $V_{1/2} = -88$ mV, $k = 8.8$; for HP) (Magee, 1998; Giocomo and Hasselmo, 2008) to obtain a somatic estimation of the biophysical conductance densities G_h* and G_{Leak}*. A summary of the calculated effective and biophysical membrane parameters is shown in Table 3.

It should be noted that similar values of the effective conductances can be calculated for the model of Table 1, by using Eqs. (10) and (11). The discrepancies in the estimated biophysical conductances G_h* and G_{Leak}* are due to the different activation curves and time constants used. As mentioned before, the system is described by the linearized parameters, and distinct configurations of biophysical properties could generate similar results. Moreover, as for the previous model, the parameters for AM cells describe the properties of the Z function but fail to reproduce the Φ profile. AM neurons are highly dissimilar in size and morphology and display a wide range of R_{in} values. Thus, considering them as part of only one main group sharing similar resonance properties may not be appropriate. On the other hand, it is possible that the magnitude of C assigned to this population was overestimated. In our approach, the value of τ_h calculated from Eq. (16), and the other parameters, are strongly influenced by the specific C value chosen to represent the whole population. Interestingly, reducing the magnitude of C, while preserving the factor $\tau_h C$ (Eq. (16)), allows a proper reproduction of the Z and Φ signatures, and the resulting G_{Leak}* approaches the values of SL and HP. A more detailed investigation of the properties of this type of resonant cells is required to evaluate this possibility. The results summarized in Table 4 agree with the prediction of an increase in g_1* in the AM-HP-SL direction and this increment is enough to compensate for the effects of a diminished τ_h. Moreover, the results are consistent with a similar G_{Leak}* among SL and HP.

Finally, it is important to add that a cell by cell analysis of the HP group in isolation revealed a positive correlation between f_R and the resonant strength Q (not shown), which suggests that the diversity in frequency selectivity inside this population also relies specifically on g_1*, and that G_{Leak}* is preserved. In addition, a higher τ_h could also contribute to an increased Q in cells with higher f_R.

(Received 10 February 2018, Accepted 31 October 2019)
(Available online 27 November 2019)